Available online at www.sciencedirect.com
SCIENCE DIRECT®
Engineering Fracture Mechanics 72 (2005) 2037–2071
Engineering Fracture Mechanics
www.elsevier.com/locate/engfracmech

The role of atomistic simulations in probing the small-scale aspects of fracture—a case study on a single-walled carbon nanotube

Qiang Lu, Baidurya Bhattacharya *

Department of Civil and Environmental Engineering, University of Delaware, Newark, DE 19716, United States

Received 16 April 2004; received in revised form 5 October 2004; accepted 17 January 2005
Available online 29 March 2005

Abstract

This paper reviews atomistic simulation (AS) of fracture of solids along with recent advances reported in the literature. While classical fracture mechanics is based on continuum assumptions, AS can provide a first-principles based description of fracture that accounts for the discrete nature of matter. The idea of atomistic simulation was first applied to fracture during the early 1970s; brittle fracture was studied first using simple potential models and equilibrium conditions. Advances in materials science and computational power have led to significant progress in AS of fracture. Since the early 1990s, complex phenomena such as ductile fracture, fracture of non-homogeneous materials, fracture interaction with other physical and chemical effects have increasingly been investigated by atomistic simulation. This paper discusses achievements and shortcomings in regard to fracture criteria, potential models, initial and boundary conditions, temperature control and multi-scale simulation. An atomistic simulation of the displacement-controlled fracture process of a single-walled carbon nanotube (SWNT) with a pre-existing Stone–Wales defect is given as an example highlighting the essential steps of the methodology. Elastic modulus, ultimate strength and ultimate strain of the tube are determined from the simulation results (both with the defect and in the defect-free case) and the dependence of these parameters on the loading rate is investigated. Time histories of potential energy, temperature, axial force and bond angle are described, and a series of snapshots detailing the progress of the fracture process is provided.

Keywords: Small scale; Atomistic simulation; Carbon nanotube; Fracture; Mechanical properties; Stone–Wales defect

* Corresponding author. Tel.: +1 302 831 4952; fax: +1 302 831 3640.
E-mail address: bhattacharya@ce.udel.edu (B. Bhattacharya).

0013-7944/$ - see front matter © 2005 Elsevier Ltd. All rights reserved.
doi:10.1016/j.engfracmech.2005.01.009

1. Introduction

In the 1950s, molecular dynamic simulation (MDS) was first introduced by physicists to study the bulk properties of matter [1]. Today the idea of simulation at the atomic or molecular level is applied in physics, chemistry, material science, biology, etc., both in academics and in the industry. In the context of simulation of fracture in solids, atoms, rather than molecules, are the primary entities. Consequently, we use the term "atomistic simulation" (AS) in this paper which is in tune with the current literature on the subject, although the basic idea is essentially the same as in MDS.

Atomistic simulation predicts the motion of a large number of atoms based on appropriate assumption of their interactive forces and boundary conditions (Fig. 1). At the heart of atomistic simulation is Newton's law $F = ma$ of classical mechanics. The simulation starts from a set of initial conditions, which basically includes the initial positions and velocities of all the atoms [2–4] and continues to monitor the state of all the atoms in the system until the loading process is complete or equilibrium is reached. Relevant quantities such as elastic modulus, fracture toughness, etc can be derived from the simulation results.

The interactive forces between atoms are commonly represented in the form of interatomic potential energy models. The potential energy is usually a function of the positions of atoms. The parameters of the model can be obtained empirically from experimental data on material properties such as elastic

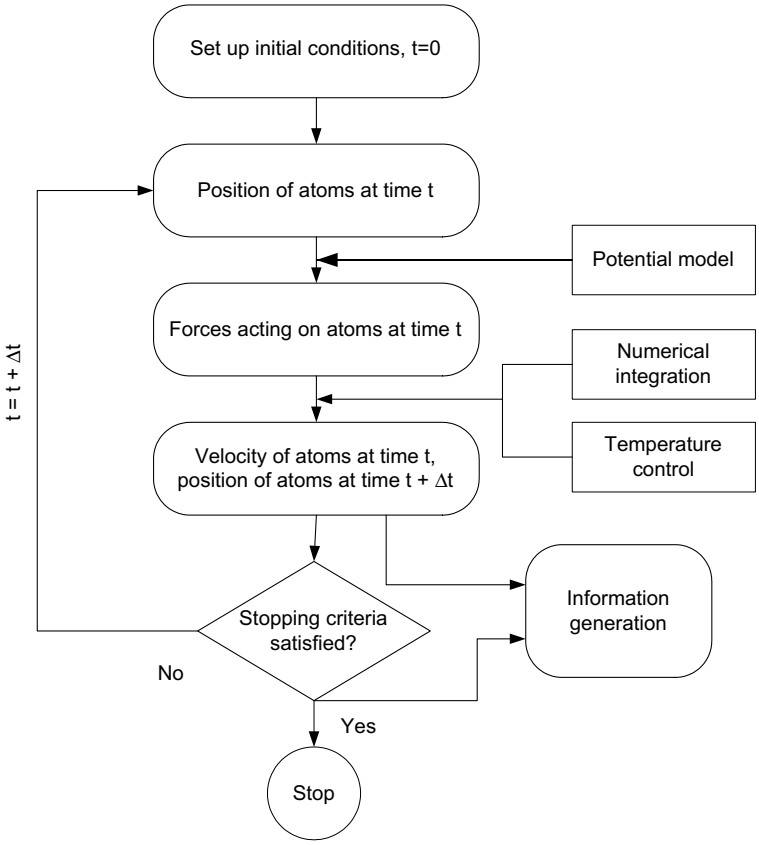

Fig. 1. Basic steps in atomistic simulation of fracture.

modulus and cohesive energies (the energy required to break the atoms of the solid into isolated atomic species). In more advanced models, the parameters can be obtained from studying the electronic structure of atoms using quantum mechanics methods.

The calculation of forces is the most time-consuming part of atomistic simulations because of the large number of atoms involved. The force on the ith atom is obtained by the differentiating the potential function, ϕ:

$$f_i = -\frac{\partial \phi(\mathbf{r}_1, \mathbf{r}_2, \ldots \mathbf{r}_N)}{\partial \mathbf{r}_i} \tag{1}$$

Although the potential, as indicated above, is a function of all the N atoms in the simulation, a truncation distance of potential model is invariably used since the summation of N-tuple potential of all particles is beyond the ability of present-day computers.

The differential equations of atomic motion

$$\mathrm{d}^2 r_i(t)/\mathrm{d}t^2 = a_i(t) = f_i(t)/m_i \tag{2}$$

are solved by numerical integration where $r_i(t)$ and $a_i(t)$ are, respectively, the position and acceleration of the ith atom at time t, and m_i is its mass. Standard integration algorithms such as Runge–Kutta algorithm or Verlet algorithm are frequently used. The latter is given by

$$r(t + \Delta t) = 2r(t) - r(t - \Delta t) + \frac{f(t)}{m}\Delta t^2 + \mathrm{O}(\Delta t^4) \tag{3}$$

The time interval Δt needs to be significantly smaller than the typical time taken for an atom to travel its own length.

The basic idea of atomistic simulation has not changed much since the 1950s. Tricks like periodic boundary conditions and potential model truncation used widely in current simulations have been used from the very beginning. However, sophisticated techniques such as temperature control, application of quantum mechanics in determining atomic interactions, parallel computation, multi-scale modeling and advanced visualization methods have gradually been introduced over the past several decades.

This paper is organized as follows. In Section 2, the shortcomings of continuum based approaches in addressing fracture are discussed, and the suitability of atomistic simulation as an inexpensive computational/experimental alternative is highlighted. Following this, the essential aspects of atomistic simulation of fracture are described in Section 3. Recent advances in regard to general mechanism of fracture, advanced simulation techniques, scale bridging, etc. are discussed in Section 4. A numerical example of fracture simulation is provided in Section 5 where a single-walled carbon nanotube with a pre-existing defect is pulled to failure under displacement controlled loading. Finally, current shortcomings and future needs in atomistic simulation of fracture are discussed in Section 6.

2. Need for atomistic simulation of fracture

Scientific research has always been motivated, among others, by a desire to explore natural phenomena at a fundamental level. The first good attempt to explain fracture phenomena physically is the famous Griffith theory. Based on the stress solution proposed by Inglis [5], Griffith [6] treated fracture as an equilibrium process in which the loss of strain energy can be equated to the surface energy generated due to the growth of cracks. The problem of singularity at crack tip was thus circumvented. His theory provided good physical background and was successfully applied to fracture of glass. Linear elastic fracture mechanics (LEFM) was developed during the late 1940s to the early 1960s. The milestones are: Irwin [7] and Orowan [8]

independently extended Griffith's theory to metals; Irwin [9] used the Westergaard approach [10] to show that the local stresses and displacements near the crack tip had a general closed form solution that could be described by a single constant, i.e. the stress intensity factor, that was related to the strain energy release rate; and the Paris–Erdogan law [11] which shows how the stress intensity factor could be effectively applied to describe fatigue crack growth. LEFM was initially focused on linear elastic-brittle behavior, thus was only applied to fracture with limited plastic deformation. The need for fracture mechanics analysis in ductile materials gave birth to elastic–plastic fracture mechanics (EPFM) in the late 1960s. Several researchers developed corrections for yielding at crack tip including Irwin [12], Dugdale [13] and Barenblatt [14]. Wells [15] proposed the displacement of the crack surface as an alternative criterion for ductile fracture, which led to the development of the parameter now known as the crack tip opening displacement (CTOD). Rice [16] introduced a parameter in a line integral form, the J-integral, to express the nonlinear strain release rate. Hutchinson [17] and Rice and Rosengren [18] related the J-integral to the crack tip stress fields in nonlinear materials. Similar concepts were developed independently by Sanders [19], Eshelby [20] and Cherepanov [21]. Begley and Landes [22] were able to establish the J-integral parameters as the premier criterion in elastic–plastic fracture mechanics. Shi and Hutchinson [23] provided the theoretical framework for establishing the relation between toughness, stress and flaw size based on J-integral concept, thus made it possible to apply to real designs. Shih [24] later showed that the J-integral and CTOD are equally valid for characterizing fracture.

The first study of rapid crack growth is perhaps Mott's paper in 1948 [25], in which he applied dimensional analysis to determine the relationship between kinetic energy and crack speed, and obtained a limiting crack speed proportional to C_0 the elastic bar wave speed for the material. Dulaney and Brace [26] and Berry [27] independently derived a crack growth history relation that corrected the error in Mott's result. In 1954, Robert and Wells [28] obtained an estimated limiting speed of $0.38C_0$ by applying the Westergaard stress function [10]. Yoffe [29] provided the first dynamic solution in 1951, which gives a limiting speed estimate of $0.6C_2$, where C_2 is the shear wave speed. Broberg [30] later improved Yoffe's solution by considering a uniformly expanding crack, and suggested the limiting speed is C_R, the Rayleigh wave speed. Atkinson and Eshelby [31] introduced the contour integral idea to account for inertia and viscoplasticity. Freund [32–34] and Nilsson [35] performed more detailed numerical analysis for unrestricted crack growth in an infinite domain, and predicted a limiting crack speed larger than Robert and Wells' result. On the experimental side, the earliest experiment for dynamic fracture might be done by Schardin's [36] in 1930s. Other important works are: the measurement of actual crack speed by Hudson and Greenfield [37] in 1947, the photoelastic investigation by Wells and Post [38] in 1958, crack growth measurements by Carlsson [39] (the interested reader is referred to the excellent texts such as [40–42] for further details).

The development of fracture mechanics over the past half century has also led to far-reaching contributions in various engineering disciplines, which is readily apparent from the multitude of fracture mechanics-based design guides and codes of practice. Examples include the Boilers and Pressure Vessels code by the ASME [43], Fracture performance tests by BSI [44], Manual for Condition Evaluation of Bridges by AASHTO [45], Fitness-For-Service of Pipings, Vessels and Tanks by API [46], Standard Test Method for Measurement of Fracture Toughness by ASTM [47], etc.

Nevertheless, in spite of their brilliant successes, LEFM, EPFM, etc. are, in essence, elegant continuum models developed from Griffith's energy balance concept. Fracture, on the other hand, is essentially the breaking of atomic bonds and crack propagation is nothing but successive breaking of atomic bonds at the crack tip. Fracture is thus significantly affected by details such as material structures and compositions at atomic level, which cannot be completely explained by continuum theories. Continuum mechanics is based on the existence of the so-called representative volume element, a necessary aspect of which is to assign properties and responses averaged over a sufficiently large volume element onto idealized material points [48–50]. Such "smoothing out" cannot occur without significant loss of information, and continuum approaches may not always be adequate when phenomena involving fracture are concerned.

For example, at the atomic scale, the discrete lattice structure gives rise to the so-called "lattice trapping" effect [51], which results in a higher fracture toughness than Griffith's theory predicts. According to the Griffith theory, the critical stress for a brittle crack to propagate is

$$\sigma_{\mathrm{F}} = \sqrt{\frac{2E\gamma}{\pi a}} \tag{4}$$

where E is Young's modulus, γ is the surface energy per unit area and a is the crack's half-length. Crack propagates if stress is greater than σ_{F}. A study with atomistic model [51], however, shows that the discrete lattice structure introduces certain constraints on the critical stress level, such that the crack does not propagate at the predicted stress value shown above, but at a higher value, called σ_+. For same reason, the stress level where crack heals is less than the predicted value, and is called σ_-. The σ_+ and σ_- are the upper and lower limit of the stress for the crack to propagate and to heal, respectively. A ratio $R = \sigma_+/\sigma_-$ was found to be 1.15 in the same study.

"Lattice trapping" also results in other effects which cannot be predicted by continuum theories, for example, the "directional anisotropy" effect [52–55]. Griffith's theory predicts that fracture is most likely to occur in the plane with lowest surface energy, and within a certain crack surface, there is no preferred crack direction. However, atomistic studies show that because the lattice trapping effect is anisotropic in nature, there is a preferred plane and direction of crack propagation. Also due to this anisotropy, the most likely crack plane can also be changed to one without the lowest surface energy, as confirmed by a few experiments [53,56,57].

In one study on tungsten [53], the fracture toughness of tungsten crystals were measured both at room temperature and at 77 K; atomistic simulations were carried out for comparison. Experiments show that with decreasing temperature, the $\langle 1\,1\,0\rangle$ direction is preferred over the $\langle 1\,0\,0\rangle$ direction for both $\{1\,0\,0\}$ and $\{1\,1\,0\}$ crack systems; this finding coincides with atomistic simulation results as well. By carefully excluding other possible reasons such as dislocation activities and mistakes in interatomic potential, the authors concluded that the anisotropy is caused by the discrete lattice structure itself.

Another study shows that directional anisotropy of cleavage fracture can also be caused by a tilted grain boundary [58]. Both effects from discrete lattice and tilt boundaries cannot be predicted by available continuum based theories without understanding the material characteristics at atomic scale.

Furthermore, the location and configuration of defects at atomic scale are random in nature, thus it is more difficult to study the effect of defects on material properties with continuum-based theories. These defects include point defects such as vacancies and interstitials, line defects such as dislocations, surface defects such as grain boundaries and stacking faults, and bulk defects such as voids and cracks. It is well known that fracture behavior is affected significantly by these defects [59]. For example, the ductile-to-brittle transition of fracture is directly related to the dislocation nucleation and mobility at the crack tip [60–62]. Although there are other available dislocation models [63], these models cannot account for the interaction of the dislocation with the crack tip without considering the atomic details at the crack tip.

It is therefore clear that fracture is naturally suited to be studied at the atomistic level. Furthermore, fracture is an environment-sensitive phenomenon: physical and chemical factors such as temperature, irradiation, electronic or magnetic fields, chemical erosions or biological erosions can largely change the behavior of fracture. Analytical methods are quite restricted in their ability to study these problems, but complex environmental effects can be handled at atomistic scales in a relatively straightforward manner by describing them as actions on each atom; a few examples are given in Section 4.1. Moreover, real experiments are difficult and often prohibitively expensive to be performed at such small scales and atomistic simulation provides a viable alternative in the form of "computational experiments". The recent interest in nano/micro-electro-mechanical systems also makes atomistic simulation an attractive platform for their design and analysis since AS is performed at a scale that is becoming increasingly compatible with the actual size of these nano/micro-systems.

3. Essential features of atomistic simulation of fracture

As early as the 1960s, researchers started to use discrete atomic lattice models to study the strain energy at dislocation core [64,65], which cannot be solved by continuum theories because of the singularity at the tip. As described above, Thomson [51] studied lattice trapping with a discrete atomic model. Although his approach was analytical, Thomson's results drew attention to the discrete nature of fracture. However, possibly the earliest simulations of fracture using atomic model were conducted by Chang [66] in his study on core structures of edge and screw dislocations in BCC and FCC iron; by Kanninen and Gehlen [67] in their study on cracks in α-iron; and by Sinclair [68,69] in his study on the BCC dislocation core and the influence of interatomic force models and kinks on the propagation of brittle cracks.

These early studies mainly focused on fracture resistance of materials. Compared with present-day simulations, simple potential models and equilibrium conditions (crack propagation was assumed to proceed slowly) were adopted. However, they did set up a new approach to study fracture that was directly based on the atomistic nature of matter.

In this section, the essential features of atomistic simulation are discussed under the context of fracture of solids. These features include the interatomic potential models, initial conditions, boundary conditions and loading methods, fracture criteria, temperature control and extraction of relevant information from the simulation.

3.1. Potential models

The mechanical, thermo-dynamical and electro-magnetic properties of a material and its structure are largely determined by the chemical bonds among its atoms. In the context of atomistic simulation for solids, interatomic forces, which are governed by the chemical bonds, are expressed in terms of interatomic potential models. An ideal potential should be able to accurately describe the interaction including the effects of valence electrons which bind the atoms together, and would require the solution of Schrödinger equation (Schrödinger equation is a wave equation describing analytically the probability of the states of electrons, the eigenvalues of the wave equation were shown to be equal to the energy levels of the quantum mechanical system). A "full" quantum simulation includes the interactions between the nuclei in each time step and the degrees of freedom of electrons are directly obtained from electronic structure, which is not applicable to a system of many atoms. Approximate approaches including tight binding [70,71] and density functional theory [72,73] have been used in such ab initio simulation of fracture.

At the present state of the art, the ab initio approach is limited by computational resources to usually a few thousand atoms. Therefore, so-called *classical potentials* (as opposed to *quantum mechanical* or ab initio) are used extensively; these classical potential models are to various extend empirical in nature and are often functions of atomic positions ($\mathbf{r}_1, \ldots \mathbf{r}_N$) alone. Although these relatively simple classical mechanics based functions provide only approximate information about the bonding of the real material, they have shown their advantages in numerous applications of fracture simulation (as detailed in Section 4) and in interpretations of the properties of materials, (e.g., [74]). In this paper, the word "potential" is used only for the potential models based on classical mechanics, no quantum mechanics is involved in the simulations.

A large number of interatomic potentials have been developed and reported in the literature; each of these models is usually tailored for use with a select group of materials. They range from the simple pair potentials, to relatively complicated potentials incorporating effects of bond angles, bond orders, local electron densities, etc.

As mentioned in Section 1, the interaction between atoms drops quickly as their separation becomes large. Thus it is computationally convenient to choose a cut-off distance, r_c, so that for a given atom, i, only those atoms within a radius r_c from i are treated as its neighbors and are involved in the calculation of its

potential. Apart from making the simulation more efficient, the cut-off distance may also play an important role in defining the bond breaking and hence the onset of fracture (discussed in Section 3.4).

The potentials used in very early stages (1950–1960s) were empirical isotropic pair potentials (Lennard-Jones potential [75] introduced in 1924, Morse potential [76] introduced in 1929, etc.). These are ideally suited for atoms with no valence electrons. For isotropic pair potentials, the total potential energy of the whole system is given by the sum of pairwise contributions within the cut-off distance:

$$E_{\text{tot}} = \sum_i \sum_{j>i} \phi_2(r_{ij}), \quad \phi_2(r_{ij}) = 0 \quad \text{for } r_{ij} > r_c \tag{5}$$

where $\phi_2(r_{ij})$ is the pairwise potential function usually in an exponential or polynomial form, and r_{ij} is the scalar distance between atoms i and j. In this class of models, the interaction among atoms is confined only to pairs and depend only on the relative spacing between the atoms (regardless of the direction). The parameters used in the potential function are obtained empirically, often by fitting predicted intrinsic material properties such as the elastic modulus and crystal lattice parameter to their experimental values. These pair potentials reflect the basic interatomic relations such as the Pauli repulsion and dipole–dipole attraction.

As an example, consider the parameters of the Morse potential for copper [77–79]. The Morse potential for metals is usually given in the form

$$\phi(r_{ij}) = D[\exp\{-2\alpha(r_{ij} - r_0)\} - 2\exp\{-\alpha(r_{ij} - r_0)\}] \tag{6}$$

consisting of three model parameters, D, α and r_0. These three parameters can be determined by fitting them to experiment data on equilibrium lattice parameter (a), cohesive energy (E_{cohesive}) and bulk modulus (B) at zero temperature and pressure. The potential energy per atom, Φ, in a cluster of N atoms is obtained by (i) choosing one atom in the lattice as the origin, (ii) calculating the sum of its interaction with all the other atoms in the cluster, and (iii) dividing the sum by 2 because all atoms have been counted twice

$$\Phi = \frac{1}{2} D \sum_{j=1}^{N} [e^{-2\alpha(r_{ij}-r_0)} - 2e^{-\alpha(r_{ij}-r_0)}] \tag{7}$$

Φ should satisfy the three conditions below.

(i) For equilibrium

$$\left.\frac{d\Phi}{da}\right|_{a=a_0} = 0 \tag{8}$$

where a_0 is the value of lattice parameter for which the lattice is in equilibrium at 0 K.

(ii) Cohesive energy per atom (the cohesive energy of a solid is the energy required to break the atoms of the solid into isolated atomic species):

$$\Phi = \frac{1}{2} D \sum_{j=1}^{N} [e^{-2\alpha(r_{ij}-r_0)} - 2e^{-\alpha(r_{ij}-r_0)}] = E_{\text{cohesive},0} \tag{9}$$

where $E_{\text{cohesive},0}$ is the cohesive energy at zero temperature and pressure.

(iii) Bulk modulus

$$B_0 = V_0 \left.\frac{d^2\Phi}{dV^2}\right|_{a=a_0} \tag{10}$$

where V is the volume of lattice occupied by one atom, V_0 is the corresponding volume at zero temperature, and B_0 is the bulk modulus at zero temperature and pressure.

Since copper has FCC structure, only the 12 nearest neighbors around one particular atom are considered in the calculation of potential energy, hence $N = 12$ and $V = a^3/4$. Using (7) in Eqs. (8)–(10), we obtain the three model parameters:

$$r_0 = \frac{\sqrt{2}}{2}a_0, \quad D = \frac{E_{\text{cohesive},0}}{6}, \quad \alpha^2 = \frac{3B_0 r_0}{4\sqrt{2}D} \tag{11}$$

The experiment data on copper and the three fitted parameters for the Morse potential (Eq. (6)) are listed in Table 1.

Isotropic pair potentials were originally developed for liquids and gases. Basically, they describe the interaction of closed-shell atoms. They were applied extensively in the early years to simulation of solids with the purpose of obtaining basic properties such as stability of lattice structure, defects in metals [80–82] and fracture behaviors [66,67]; etc.), and they continue to be in use today mainly because of their simplicity [83]. Isotropic pair potentials can give good results if applied properly, but they suffer from major shortcomings when applied to solid metals. For example, the melting temperature, the vacancy formation energy and the ratio of the elastic constants, C_{12}/C_{44}, of a cubic crystal generated by pair potentials cannot fit the corresponding experimental data [84,85]. The reason is that these models have no environmental dependence, making little difference between behavior of a bulk atom and that of a surface atom. Studies have shown the electron density effects are necessary for correct simulation of metals [84,86,87].

Many-body potentials consider the effects of local electron density. Examples include the embedded atom method (EAM) potential [88–90], the Finnis–Sinclair [85] potential, the Sutton–Chen potential [91], etc. These potentials have the general form

$$E_{\text{tot}} = \sum_i F(\rho_i) + \sum_i \sum_{j>i} \phi_2(r_{ij}) \tag{12}$$

The term $F(\rho_i)$ is intended to model the interaction between atom i and its neighbors as a function of the local electron density where the atom i is placed. The term $\phi_2(r_{ij})$ has the same meaning as pair potential above. The functions $F(\rho_i)$ and $\phi_2(r_{ij})$ are approximately determined by studying the lattice constant, elastic constants, vacancy-formation energy and sublimation energy in various phases. This type of potential is widely used for metals due to its straightforward form and its ability to incorporate the approximate variation of bond strength with the electron density [92].

However, neither isotropic pair potentials nor many-body potentials account for the angle between atomic bonds, thus they cannot reflect the directional preference of bonding, which is essential in simulation of covalent materials and some properties of defects in metals. The Stillinger–Weber [93] potential for silicon has a two-body term and a three-body term

$$\phi(\mathbf{r}_1, \mathbf{r}_2, \ldots \mathbf{r}_N) = \sum_i \phi_1(\mathbf{r}_i) + \sum_i \sum_{j>i} \phi_2(\mathbf{r}_i, \mathbf{r}_j) + \sum_i \sum_{j>i} \sum_{k>j>i} \phi_3(\mathbf{r}_i, \mathbf{r}_j, \mathbf{r}_k) \tag{13}$$

Table 1
Morse potential parameters (determined by experimental data from [194])

Lattice parameter (Å)	Bulk modulus (dyn/cm^2) $\times 10^{12}$	Cohesive energy (eV/atom) $\times 10^{22}$	α (Å^{-1})	r_0 (Å)	D (eV)
3.61	1.37	3.49	1.41	2.55	0.582

where the two-body term accounts for the bond stretching; the three-body term manages the bond angle preference. $\mathbf{r}_i$, $\mathbf{r}_j$ and $\mathbf{r}_k$ are atomic position vectors. It reproduces well the diamond-cubic structure and liquid state of silicon. However, it is not good for modeling the amorphous solid state or under-/over-coordinated silicon atoms. Thus its validity of applications on fracture studies, where new crack surface is created, should be verified further. An example of this three-body type of potentials, which is modified from the Morse potential by adding a three-body term, has been used in a simulation of carbon nanotube in Section 5 of this paper.

The more complicated bond order potentials, including Tersoff and Brenner's models [94–96], involve the variations in bond energy due to the changes to an atom's coordination number (number of neighboring atoms). It has the form

$$E_i = \sum_{j(\neq i)} [V_R(r_{ij}) - B_{ij} V_A(r_{ij})] \tag{14}$$

where B_{ij} is the bond order term, which itself is the function of the atom's coordination number. The bond order potential is widely used for simulation the bulk and surface properties of silicon and carbon, including defects production, film growth, ion bombardment and fracture. The parameters of the functions present in these potential models are chosen primarily by fitting them to the cohesive energies of various polytypes, along with the lattice constant and bulk modulus of semiconductors. The bond order models are among the most frequently used potentials for semiconductors. However, as pointed out by a few recent studies [97,98], they do not reproduce fracture properties well and seem to give unrealistic high fracture strains.

The environment dependent interatomic potential (EDIP) [99–102] models for silicon and carbon are obtained by fitting the parameters to the cohesive energy curves obtained by ab initio calculations, but not the experimental data. They are a little more complicated than bond-order models and have the form of similar to the Stillinger–Weber potential

$$E_i = \sum_j V_2(R_{ij}, Z_i) + \sum_{jk} V_3(\vec{R}_{ij}, \vec{R}_{ik}, Z_i) \tag{15}$$

where Z_i is the coordination number of the ith atom. The pair functional $V_2(R_{ij}, Z_i)$ represents the strength of bond (ij), while the three-body functional $V_3(\vec{R}_{ij}, \vec{R}_{ik}, Z_i)$ represents preferences for special bond angles, due to hybridization, as well as the angular forces that resist bending away from those angles. The environmental effect is represented by the number of nearest neighbor atoms, which is determined by an effective coordination number Z_i for atom i. The form of this potential is derived by inversion of cohesive energy from ab initio calculation. Then by analyzing the elastic properties of covalent solids, they explored the cohesive forces in certain special bonding states. Although it is developed for bulk studies of silicon, it is also used for simulation of fracture [103].

Generally speaking, potentials are developed for targeted materials and targeted properties. Therefore, how sophisticated a potential is and what its capabilities are depend on which material is being studied and which properties one is interested in reproducing. It should also be mentioned that different potential models may be selected for the same material when simulating such diverse processes as static brittle fracture, dynamic fracture, ductile fracture and fracture with defects.

3.2. Initial conditions, boundary conditions and loading methods

Atomistic simulation predicts the time history of atomic movements by solving their differential equations. Initial conditions provide the information for the simulation to start. The initial atomic positions are determined either by their lattice structure and composition, or by random method, depending on whether the system to be simulated is crystalline or amorphous. The initial velocities are determined by

the temperature of the system, and calculated from random distributions given by statistical mechanics. Simulation of fracture usually focuses on a region around a pre-existing crack tip, assuming the crack to be of macroscopic size. The crack is described with a crack plane and a crack direction. The initial configuration of the pre-existing crack tip can be determined by a few methods: (i) simply removing several layers of atoms from the matrix, (ii) shifting the atoms on the crack surface from their original position on the crystal lattice to the position that is specified by the anisotropic elasticity continuum mechanics equations [104] for a desired value of the stress intensity factor.

Periodic boundary conditions are widely applied in many simulations of gases and liquids in order to avoid free surfaces. The basic idea is to replicate the simulation cell infinitely in all directions, thus these replicas serve as the boundaries. However, this method causes problem in fracture simulations since the crack is not periodic in all directions. Under the periodic assumption, the crack and the related defects would interact with themselves ad infinitum, which would result in fictitious forces and energies. Therefore, in most fracture simulations, a boundary layer of atoms is defined to serve to reduce the edge effects and maintain proper configuration of the lattice [66–68]. Fig. 2 shows boundary layers as shadowed circles in an example of Mode II fracture with a pre-existing crack.

Mechanical load can be applied through one or more layers of the boundary atoms, by prescribing either the displacements [105–107] or forces [108–110] on the boundaries. The loading strategy in Guo et al.'s study [111] is shown as a typical example: (i) before applying the external loading, the interior atoms are relaxed to reach equilibrium. (ii) The external loading is applied incrementally, by moving the boundary atoms according to the linear-elastic solution. (iii) The boundary atoms further interact with the interior atoms. For a specified stress intensity factor, the system is relaxed under fixed-displacement boundary condition for several hundred time steps. (iv) The stress intensity factor is updated during the simulation due to the change of crack size. The load is incrementally applied by repeating the above procedure.

Special loading methods may be applied to simulate fracture in the presence of electric field, magnetic field, radiation, chemical erosion, etc. (brief examples are given in Section 4.1).

With increasing computational resources, the number of atoms in recent simulations have reached the order of 10^9 [112,113], which is nevertheless still many orders of magnitude less than the representative volume element of the material. Thus the simulations invariably focus on the neighboring area around the crack tip. Therefore, the size of the material under study is always not large enough, so that the properties obtained from the simulation cannot reflect the general properties of the material correctly. In some studies, this problem is solved by integrating different sizes of models in one simulation, which is popularly called multi-scale modeling (introduced in Section 4.2).

3.3. Temperature control

In conventional atomistic simulation, instantaneous temperature T of the system is calculated based on the statistics of the particle momenta [2]:

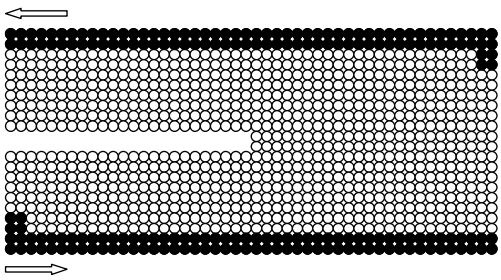

Fig. 2. Geometry and loading method for Mode II crack.

$$T(t) = \sum_{i=1}^{N} \frac{m_i v_i^2(t)}{k_B N_f} \tag{16}$$

where $T(t)$ is the instantaneous temperature at time t, m_i is the atomic mass, $v_i(t)$ is the atomic velocity at time t, k_B is the Boltzmann constant, N is the number of particles, N_f (=$3N - 3$) is the degree of freedom.

The original idea of molecular dynamics simulation was developed to study the natural time evolution of an isolated system of N particles occupying a volume V and with total energy E. In statistical mechanics, these systems belong to the *microcanonical ensemble*, or NVE ensemble; the temperature is not constant for *NVE* ensemble. However, constant temperature is sometimes a favorable feature in simulations with net energy input/output, such as mechanical loading in fracture simulation. Without any control, the temperature of the system could go unrealistically high or low. The systems with constant temperature belong to the *canonical* ensemble, or *NVT* ensemble, in which the particle number N, the volume V and the temperature T are constant.

An ideal temperature control technique should have control on the velocities of all particles so that they obey the distribution for canonical system at a given temperature; also, the trajectories of particles (velocities and positions) should be ergodic, that is, the ensemble average can be replaced by the temporal average.

Various techniques for temperature control have been frequently used. The widely used *Nose–Hoover approaches* include the original Nose Hamiltonian [114], the Nose–Hoover dynamics [115], the Nose–Hoover chains [116], and other modifications [117,118]. Basically the idea in the Nose–Hoover approaches is to add one additional degree of freedom to the system that acts as a heat reservoir. It controls the fluctuation in the system temperature by controlling the heat flux between the reservoir and the system. The *velocity rescaling* method simply rescales the atomic velocities to attain the desired temperature [4]. The *Anderson thermostat* [119] couples the system to a heat bath that is represented by stochastic impulsive forces acting occasionally on randomly selected particles. These stochastic collisions with the heat bath simulate the energy exchange between the system and the heat bath. The Gaussian thermostat, based on Gauss' principle of least constraint, is to project the particle momentum to the iso-kinetic hyperspace [120].

Generally speaking, temperature control techniques can be very helpful but they must be applied carefully so that the artificial modifications introduced to the atomic velocities are physically meaningful. However, temperature control techniques are not guaranteed to work well in non-equilibrium situations [121]. It is therefore necessary to understand their limitations before using them arbitrarily in fracture simulation which can be a highly non-equilibrium process.

3.4. Identification and detection of fracture

At the macroscale, "fracture" can be defined as the growth of a single dominant crack (or a group of cracks) leading to the separation of a member into two pieces usually under the application of loads. At the atomic scale, however, fracture is simply the breaking of a series of atomic bonds. Therefore the criterion for atomic bond breaking has to be clarified for atomistic simulations.

In most studies, crack extension is detected either by observing the distance among atoms or by direct inspection of the configuration of the atomic arrays. If the separation between a pair atoms exceeds a critical distance (call it r_f), where the interatomic force drops close to zero, the bond between the atoms is regarded as broken. Fig. 3(left) shows an 2-dimensional picture of a local area around a brittle crack tip. Dots denote atoms, a crack is drawn with dashed lines. Fig. 3(right) shows the three atoms closest to the crack tip. The separation between atom B and C is less than r_f, which means the bond between them remains unbroken. The separation between atom A and C in Fig. 3(right), on the other hand, is greater than r_f, so the bond between them is regarded as broken. It may be necessary in some investigations to identify the precise location of the crack tip (e.g., in deriving fracture toughness) which nevertheless is somewhat

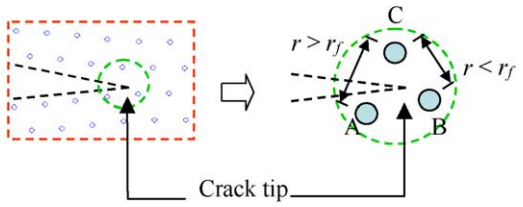

Fig. 3. Distance-based fracture criterion at atomic level.

arbitrary at the atomic scale. One can definitely conclude in the above example that the crack tip is somewhere within the triangular region ABC since the crack extends to the right of atom A but falls short of atom B, yet the exact position of the tip cannot be defined without making additional assumptions.

The above approach can be summarized as *distanced-based* detection, and is used widely in atomistic studies of fracture [55,122–126], although not every study mentions the specific value of r_f. Generally, a good guess is that r_f is associated with the cut-off distance (r_c) of potential energy functions (refer to Section 3.1), since the cut-off distance is where the interatomic force drops close to zero.

Rebonding of atoms is important in simulations of formation of dislocations and healing of cracks. Generally, rebonding is defined with the same method as bond breaking. For example, in the fracture simulation of α-iron by Machova and Kroupa [123], the cut-off distance r_c is as criteria for both crack extending and healing. That is, when the distance between individual atoms r exceeds the cut-off distance r_c, the bond is regarded as broken; when $r < r_c$ the bond is regarded as healed. However, in a few cases, particularly for studying dynamic fracture [83], rebonding is forbidden, basically to simplify the problem.

Other than crack extension and healing, the study of characteristic phenomena, especially defects, are important for fracture studies. *Energy-based* detection methods can be used to monitor these important features. Since the atoms at equilibrium position has lowest potential energy, atoms associated with defects or crack surface are characterized by their high potential energies. Therefore, by monitoring potential energies of individual atoms, it is possible to detect defects and crack surface [127]. For example, atoms with potential energies greater than 97% of the equilibrium value of the atomic potential energy (negative in this study) are highlighted as atoms involved in a dislocation, microcrack or other imperfections in a study by Abraham et al. [113]. The method has advantage especially when large number of atoms are involved, or when ductile behavior is of special importance.

3.5. Extraction of relevant information

Atomistic simulation essentially tracks the time evolution of the positions and velocities of the atoms. From this basic information and using relevant geometric and loading characteristics, further quantities can be generated as described below.

The geometry of the crack tip, evolution of point defects, movement of dislocations, crack speed, vibration frequencies and modes, etc. can be obtained by directly monitoring the atomic positions and using the methods of detecting fracture and defects discussed in Section 3.4.

Temperature of the system (Eq. (16)), forces, potential and kinetic energies of individual atoms, thermoconductivities, elastic modulus, fracture toughness, etc. can also be calculated from the basic information. For example, in the simulation of carbon nanotube, the Young's modulus and the Poisson's ratio were calculated, respectively, using the classical relations $E_z = \sigma_{zz}/\varepsilon^0_{zz}$ and $\nu_{z\theta} = -\varepsilon_{\theta\theta}/\varepsilon^0_{zz}$ by [128], where σ_{zz} is the axial stress, ε^0_{zz} is the axial strain and $\varepsilon_{\theta\theta}$ is the radial strain.

Stress calculation is often used in atomistic simulations of fracture. However, it is important to note that the concept of stress is originally defined in the context of continuum mechanics. At the atomic level, force,

rather than stress, is the more natural measure of mechanical interaction. To connect atomic systems with continuum-based analysis, several methods of measurement of stress at the atomic scale are developed.

Stress has sometimes been computed using the classical result from thermo-mechanics as the strain derivative of the elastic strain energy (e.g., [129])

$$\sigma = \frac{1}{A}\left(\frac{\partial E_S}{\partial \varepsilon}\right) \tag{17}$$

where E_S is the elastic strain energy, ε is the strain, A is the cross-sectional area. Another widely used stress definition is based on a generalization of the virial theorem of Clausius [130] for gas pressure. The average virial stress over a volume Ω around a particle i at position $\mathbf{r}_i$ is

$$\overline{\Pi} = \frac{1}{\Omega}\left(-m_i\dot{\mathbf{u}}_i \otimes \dot{\mathbf{u}}_i + \frac{1}{2}\sum_{j\neq i}\mathbf{r}_{ij} \otimes \mathbf{f}_{ij}\right) \tag{18}$$

where m_i is the mass of atom i, $\mathbf{u}_i$ is the displacement of atom i relative to a reference position, the superscript dot indicates material time derivative (which is the Eulerian expression of the rate of change of any property of a fluid particle as it moves through the flow field), $\mathbf{r}_{ij} = \mathbf{r}_j - \mathbf{r}_i$ and $\otimes$ denotes tensor product. Applying the continuum equation of balance of momentum, Lusko [131] derived a similar expression for stress in a form suitable for atomistic simulations. The stress expression has two parts, a kinetic part depending on the mass and velocity of atomic particles, reflecting an assertion that mass transfer causes mechanical stress to be applied on stationary spatial surfaces external to an atomic-particle system; and a potential part, depending on interatomic forces and atomic positions, providing a continuum measure for the internal mechanical interactions between particles. The virial expression of stress was originally defined for gases and liquids, and was later extended to solids (mainly homogeneous solids in equilibrium). Obviously, it cannot reflect the effects of local defects or deformations when their contributions are averaged over the whole volume. Eq. (17) derived from strain energy suffers from the same problem. Tsai [132] has shown that the virial stress definition can also be expressed by accounting of all the forces acting across an appropriate surface

$$\sigma_i = \frac{1}{A}\sum_i \frac{m_i|v_i|}{\Delta t} + \sum_R X(j,k) \tag{19}$$

where A is the area of the surface, $X(j,k)$ is the force exerting from one side of the surface to the other side, i denotes atoms which cross the surface during Δt. This definition was proved to be the physically same as the virial stress defined on a volume when applied to homogeneous bodies, and is favored generally for simulation of solids since it can give the local stress variation in the region of an atomic-level inhomogeneity [132–134]; see Zhou and Shi 2002 [135] for an example involving carbon nanotubes.

Although these methods (Eqs. (18) and (19)) are widely applied, according a recent paper by Zhou [136], they contain weak points in (i) defining the concept of stress in systems with discrete nature and (ii) confusing the material and spatial balance of momentum. Zhou claimed that the virial stress is actually not a measure of mechanical stress. Instead, the interatomic force term itself in the virial form is a valid stress measure and can be identified with the Cauchy stress. This study seems to be an important revision to the measurement of stress in atomistic simulations for mechanical properties.

In the numerical example in Section 5, axial stress σ_{zz} is calculated as

$$\sigma_{zz} = \frac{F_z}{A} \tag{20}$$

where F_z is the axial force measured on one end of the specimen, A is the cross-sectional area. This is intended to measure the instantaneous far-field stress in the tensile specimen instead of a volume averaged quantity. This approach has also been adopted by a few other studies [137–139].

Apart from mathematical calculations, good visualization techniques are not only helpful but also necessary to effectively explore the fracture behaviors generated by simulations, especially as the number of atoms increases to billions. Digital movies and virtual environments provide direct insight into the rich diversity of fracture phenomena [83,112,113,140].

4. Recent advances in atomistic simulations of fracture

Section 2 highlighted some of the shortcomings of continuum based modeling of fracture and outlined how atomistic simulation can be more attractive and powerful in investigating some aspects of the fracture process in solids. We now review some of the recent advances in atomistic simulation of fracture, namely in the studies of brittle, ductile, dynamic fracture mechanisms, in fracture occurring in different environments, and in the area of multi-scale simulations.

4.1. General mechanism of fracture

As already mentioned, atomistic simulation was first applied to the study of static brittle fracture in the early 1970s. With increasing computational power and advances in materials science, AS found its application in more complex phenomena including ductile fracture and dynamic fracture. Since the early 1990s, a veritable explosion of AS results have been reported in the literature: on the one hand these include predictions of new phenomena not supported by existing theories, and first-time ''experimental'' verification of long-held analytical predictions on the other.

By the early 1970s it was known that special effects such as lattice trapping cannot be predicted by continuum models. The phenomenon of directional anisotropy (discussed in Section 2) that makes a crack extend in a plane and in a direction not preferred by continuum theories has been studied more recently with AS [52–55]. Another effect of lattice trapping, ''meta-stable cracks'' in which cracks take zig-zag paths instead of smooth ones (that have the lowest surface energy) have also been studied by atomistic simulation [141,142].

One of the most challenging topics in fracture mechanism is a given specimen's preference between brittle and ductile failure modes. Why does a material break in a brittle (or, alternately, ductile) way but not the opposite? At what conditions does the brittle (or, ductile) behavior dominate? How does plasticity increase the material toughness? In the atomic scale, the transition from brittle to ductile behavior occurs when dislocations are emitted from the tip of an existing crack, and its movement causes crack blunting. A series of analytical studies have been carried out to model this process. In an early model (1974), Rice and Thomson [60] used the elasticity solutions for a fully formed dislocation ahead of the crack tip, and introduced a core cut-off radius to derive a force balance for the dislocation to move away. They gave the critical condition of the stability of the crack as $Gb/\gamma = 7.5$–10, where G is the shear modulus, b is the Burgers vector of dislocation and γ is the surface energy of the material. The shortcomings in this model were later pointed out by Rice in 1992 [62]: (i) the core cut-off distance in [60] was poorly defined, and (ii) instead of the fully formed dislocation in [60], only an incipient one actually existed prior to the instability ahead of the crack tip. In the improved model [62], Rice involved describing the incipient dislocation based on the atomic considerations within the framework of the Peierls model. He compared the energetic ''cost'' of creating new surfaces within the crystal (the surface energy γ_s) with the energy barrier that must be overcome to allow atomic planes to slip over one another (the unstable stacking fault energy γ_{us}). Rice used fracture mechanics to perform a straightforward analysis, and found that a critical ratio of these energies separates ductile from brittle behavior for a particular crystal-

lattice type and orientation. This model has since been widely used; some drawbacks has recently been argued in [143]. Rice's Peierls model has been verified with AS in a limited way [127,144] since the reproduction of dislocation emission at the crack tip and the blunting of crack tip involved in dynamic fracture required the simulation of millions of atoms and requires vast computational power.

Nevertheless, quite a few studies have also showed that Rice's Peierls model [62] is inadequate in explaining the choice of brittle vs. ductile failure mode. For examples, Zhou et al. [145,146] found that Rice's model is quite accurate for Mode II fracture, but for Mode I fracture, the ductile–brittle crossover is independent of γ_s, and is only determined by γ_{us}. Zhou et al. [127] also found that Rice's Peierls model underpredicted the critical load for dislocation emission. Based on their own simulations, Knap and Sieradzki [147] claimed that the discrepancy between simulations and Rice's Peierls model is due to the influence of the surface stress. However, simulations conducted by Farkas [144,148] showed that cleavage can happen after dislocation emission from the crack tip if the dislocations are not allowed to reach their equilibrium positions. Farkas' simulation shows that the shielding effect of the emitted dislocations decreases the total stress intensity factor at the crack tip but also causes a net decrease in the Mode II stress intensity factor projected on the slip plane of the emitted dislocations. The lower stress intensity factor along the slip plane limits the emission of new dislocations. That complex effect leads to a combined dislocation emission-crack propagation failure process.

An alternative to Rice's Peierls and Rice and Thomson's models [60,62] was provided by Hirsch et al. [61]. This analytical model states that dislocations are emitted by sources activated by the high stresses at or near the crack tip and the rate at which they move away from the crack tip determines the material toughness. Cleri et al. [109] calculated the corresponding energy release rate for cleavage, G_{cleav} and for dislocation nucleation, G_{disl} They found that G_{disl} is much smaller than that calculated by the Rice's Peierls model based on γ_{us}, but quite close to the value predicted from the energy barrier of dislocation motion which implies that the model of Hirsch et al. [61] can better explain the preference between brittle and ductile failure modes.

Atomistic simulations have also confirmed that the plasticity of bulk bodies and the mechanism of brittle-to-ductile transition are mainly controlled by the dislocation motion so that the interactions among dislocations and other defects are key factors. A model developed by Khantha et al. [149,150] explains that the sudden transition is due to the cooperation of a large number of dislocations at the crack tip. Massive dislocations lower the effective moduli and give rise to more dislocations. Therefore, above a critical temperature, T_c, the total energy of many loops becomes negative and a sudden unstable expansion of the loops takes place. Thus yielding can occur at this stage even in crystals which are initially dislocation-free. However, we have not found any atomistic simulation examples related to this method, possibly because of the massive computational demand to model a large number of dislocations.

In the area of dynamic brittle fracture, properties such as the critical load for dynamic crack initiation, the dynamic fracture toughness, etc. have been studied by AS (e.g., [125], etc). More interestingly, atomistic simulation has also been able to demonstrate a few phenomena that continuum theories did not predict. For example, continuum theories typically assume that cracks are smooth, and the limiting speed for crack propagation is the Rayleigh speed (which is the speed of sound on a solid surface) since the strain energy release rate approaches zero at Rayleigh speed. However, a recent laboratory experiment shows that Mode II crack can travel at a speed even greater than shear wave speed [151]. Moreover, laboratory experiments report that Mode I crack is initially smooth, but begins to generate branches and become misty when the crack propagates at a speed beyond 1/3 of the Rayleigh speed. Atomistic simulation [152] has shown that the flattened spatial distribution of the stress at crack tip at 1/3 Rayleigh speed induced the above instability. By artificially introducing a weak path, Abraham et al. [83] simulated the supersonic Mode II crack, and showed that the forbidden zone beyond Rayleigh speed is overcome when a transonic "daughter crack" is generated beyond the original crack, and a supersonic "granddaughter crack" is further generated beyond the "daughter crack".

Besides investigating the nature of fracture mechanisms, atomistic simulation is also particularly effective for studying fracture when atomic-scale heterogeneous materials are present or when other physical/chemical effects are involved. Examples include semiconductors subjected to a combination of mechanical and electrical loads, materials subjected to radiation [153], metal embrittlement due to hydrogen and copper [154,155], hydrogen storage of carbon nanotubes [135], etc. Such physical and chemical effects can be represented as interaction among atoms, ions, or molecules. For example, radiation damage initiation can be simulated as a transfer of a very large kinetic energy to a single atom (primary knock-on atom) [153,156]. The effect of hydrogen embrittlement can be introduced by a potential model containing the effect of hydrogen atoms, for example, a modified Morse potential for Fe–H was adopted in [154], and Brenner's bond order model was used to describe carbon–hydrogen interaction in [96]. A simulation of the oxidation of aluminum nanoclusters has been performed [157] in which the interaction scheme can account for bond formation and breakage and changes in charge transfer as atoms move and their local environments are altered. Thus this model has potential for use in the simulation of fracture under corrosive environments.

A simulation of the oxidation of aluminum nanoclusters has been performed by carefully choosing the interaction scheme [157]. This scheme is capable of treating the bond formation and breakage and changes in charge transfer as atoms move and their local environments are altered. Thus this model has potential for use in the simulation of fracture under corrosive environments.

4.2. Computational advances

Besides the advances in materials science, the development of the computational aspects of atomistic simulation is also quite notable. The widespread interest in AS in the 1990s was possible because of the rapid development of computers, especially the parallel computing technique. Atomistic simulation is inherently suitable for parallel computation [158]. The most time-consuming part of AS is the computation of the interactive forces involving many particles which can be easily divided into many small groups and assigned to individual processors working in parallel. Many general-purpose simulation programs include parallel computation techniques, such as Moldy [159] and NAMD [160] and. Parallel computation methods have also been used widely in atomistic simulation of fracture.

Although the number of atoms tackled in a given simulation keeps increasing each passing year (the limit was about 10^9 in 2002 using parallel computation [112,113], this is still orders of magnitude lower than that constituting a macroscopic representative volume element. Moreover, complicated phenomena such as fatigue (dislocation nucleation and entanglement from an atomistic view) occur over periods of time that are typically several orders of magnitude higher than the duration commonly simulated. It is therefore clear that pure atomistic simulation, without the help of scale-bridging techniques, is still severely restricted by available computational resources to model phenomena that occur over realistic intervals of space and time, and will continue to be so for years to come.

To overcome this limitation in spatial scale, two general types of methods have been proposed to connect continuum models with atomistic models. One can conduct simulation at the smallest scale of interest, extract relevant quantities, then use them to determine the parameters of the next larger-scale model, and in this way continue to integrate scales upward. Alternatively, one can describe the material process with different models in separate regions, and link them through carefully set boundary conditions, in the so-called "concurrent multi-scale simulation method". The latter approach is favored in fracture study because by carefully crossing different scales, one can study the material behaviors at macro-scale, while keeping the details at atomic scale where it is needed, such as crack tips. Various models have been used for the atomic-scale region simulation, such as Green's function and Monte Carlo simulation [161,162]. However, mainstream multi-scale simulation algorithms involve the coupling of finite element (FE) method and atomistic simulation, and we focus on only this approach in this section.

The key to multi-scale crossing is to deal with the information exchange between simulation regions at different scales through an appropriately defined interface. This information exchange, according to Nieminen [162], has to be "physically meaningful, mathematically consistent, and computationally efficient". To be specific, a multi-scale simulation involving FE and AS should ideally have the following properties: (i) The displacement at the interface connecting the two regions should coincide, this is usually done by scaling the finite element down to the atomic scale and connecting the each element node with an atom. (ii) Energy should be described correctly throughout the body, including the interface. One common method is to add a pad of atoms outside the AS region, so that the atoms at the interface feel like bulk atoms but not surface atoms. (iii) Forces for both models should be described correctly at the interface. A general problem in the coupling of AS and FE regions is that the stress/force description in the atomic lattice is non-local but in continuum model it is local [52,169,164]. In other words, at the interface of AS and FE regions, the motion of atoms in the FE region (connecting with nodes) will affect the energy in the AS region since the interatomic force has a finite range, but the motion of atoms won't change the energy of FE region. This mismatch in describing the potential energy usually causes unphysical forces (so-called "ghost forces") at the interface. (iv) The interface should allow the vibration waves and defects to pass. (v) FE elements near the interface should reflect the discrete nature of the lattice. Several popular coupling algorithms are discussed below with emphasis on how well they meet the above challenges.

In 1991, Kohlhoff et al. [52] introduced a transition region between FE meshes on the continuum side and an atomistic simulation region around the crack tip, in what is now referred to as the FEAt method. The local/non-local mismatch was solved by describing the continuum region with Kroner's non-local elasticity theory [163]. In the transition region, finite elements are scaled down to the atomic scale; the atomic lattice and the continuum overlap and each atom coincide with one element node. FE and AS regions provide displacement boundaries for each other, and the problem of the AS region and the FE region are solved separately in the two regions in an iterative way in the original paper, although a simultaneous solution is also possible as pointed by other researchers [164]. This method has drawbacks that the energy for the whole system is not conserved since the energy of atoms and the FE node they coincide with is calculated twice. The atomistic characteristics of the finite elements near the interface are not considered either. Finally, defects such as dislocations cannot pass from one region to the other.

The quasi-continuum method (QC) [165–169] uses a transition region between the FE and AS regions that conserves energy. The original QC method [165] chooses representative atoms (or "repatoms") throughout the whole body, makes FE nodes coincide with them in the continuum region, and makes every atoms in the AS regions as repatoms. In the continuum regions, the Cauchy–Born rule is applied, by which the energy of an FE element can be approximated as the energy of a typical atom within the element multiplied by the number of atoms in the element, provided the deformation is uniform. Thus the energy of the two regions can be unified and minimized at the same time. However, this approach suffers from the so-called "ghost forces", introduced by local/non-local mismatch, as mentioned in the above paragraph. Also, since the Cauchy–Born rule assumes that these atoms see uniformly deformed bulk environments, it cannot accurately describe the energy where deformation gradients changes or on surfaces. In order to solve these problems, the surface problem can be solved by making surface atoms non-local, and the "ghost forces" have later been corrected by adding counter-forces, as pointed by Shenoy [166].

However, Knap and Ortiz [168] later proposed a modified QC approach (fully non-local QC) which inherently does not have the local/non-local mismatch problem. Their basic idea is to systematically coarsen an atomistic description by the kinematic constraints provided by FE calculation. A number of FE nodes are chosen from the real atomic lattice. Around each node, a small cluster of atoms is selected, and their displacements are calculated by interpolating the displacements of the FE nodes. The atom clusters are used to calculate the nodal forces or energies, which in turn are used to find the equilibrium of FE nodes. The equilibrium of whole body is thus approached gradually. In the regions where details of atomic level are needed, every atom is chosen as a node. This method discards the Cauthy–Born rule and truly realizes a

seamless integration between the atomistic and continuum regions. However, it has several times more degrees of freedoms than the local QC, it also has the problem of overestimating surface effects of energies of elements. Miller and Tadmor [169] combined the original QC and the fully non-local QC by choosing the repatoms to be local or non-local according to their deformation environments. A treatment of a non-local treatment of a repatom is triggered by a significant variation in the deformation gradient on the atomic scale in the repatom's proximity.

Abraham and Broughton [170] included a quantum mechanics based ab initio simulation region at the crack tip, combined it with the surrounding atomistic simulation region, and, in turn, embedded the atomistic simulation region in the FE mesh (named as "coupling of length scales" or CLS method). They introduced two "hand-shaking" regions to connect the three regions. An example of fracture in silicon slab is provided. Nakano et al. [112] also discussed the seamless combination of continuum mechanics, atomistic simulation and quantum mechanics, and the applications to fracture simulation, using a similar hand-shaking algorithm as Abraham and Broughton's. Basically, their approaches follow the similar principle with local-QC method, thus, they are expected to have the same nonphysical effects induced by local/non-local mismatch.

All of the algorithms introduced above do not consider the defects after they pass into the continuum region, nor do they consider the possibility of the movement of the defects back into the AS region. The "coupled atomistic and discrete dislocation" or CADD method [171] considered this problem by dividing the continuum problem into two complementary problems: Problem I consists of discrete dislocations in an infinite elastic continuum and is solved by superposition of the analytical elastic fields due to the individual dislocations. Problem II is treated as a standard continuum-atomistic multi-scale simulation (using, say, QC, FEAt or CLS, etc.), and when superimposed with Problem I, the desired boundary conditions imposed on the continuum problem are satisfied exactly. Problem II thus consists of a linear elastic continuum with no dislocations. A detection band is defined in the AS region close to the interface, monitoring the change of strain. Once a dislocation is identified, it is passed into Problem I as a discrete dislocation. Although certain problems exist in the original study [171], such as ghost forces and the extra energy by double counting the overlapped material in transition region, this approach is unique in dealing with defect passing, and its shortcomings can be easily solved by introducing the advances of other approaches for Problem II.

However, all methods listed above are inherently "static", without considering the effects of atomic vibrations. CLS and QC methods have been extended to zero temperature dynamics, by interpolating the velocities at the FE nodes, but they have intrinsic problems when extended to finite temperature. Dynamic simulation would be the new challenges of multi-scale simulation in coming years.

The time scale bridging is even more challenging. Ordinary atomistic simulations are usually limited to nano-seconds or less since the time step in the simulation has to be small enough to guarantee accuracy. Acceleration methods, such as Voter's hyper-MD method [172,173], and the temperature-accelerated dynamics (TAD) method [174] are developed from the transition state theory (TST) [175] which characterizes the system dynamics as a sequence of infrequent transitions from one potential state to another, and the states are divided by relative high energy barriers. The basic idea of hyper-MD is to modify the potential energy surface, $V(\mathbf{r})$, by adding a bias potential, D, to the true potential such that the potential surfaces near the minima are raised and those near the barrier or saddle point are left unaffected. This is to enhance the rate of state transition while keeping the ratio of transition to any two adjacent states unaltered. Therefore, at an accelerated pace, the system evolves from state to state in a sequence representative of the exact dynamics. The temperature-accelerated dynamics (TAD) method by Sorensen and Voter [174] is similar. Instead of modifying the potential model, it starts with an atomistic simulation in some state at a higher temperature to find transition pathways, and simultaneously records the statistics of waiting times of state transitions at high temperature. According to the TST theory, the correct distribution of waiting times at original temperature can be extrapolated. Then the whole procedure is repeated in the new state, and in this way the system is moved from state to state. The major advantage of both methods is time economy. It is

said that hyper-MD method can extend the simulation time scale by 2 or more orders of magnitude [172,174]. However, both method are built on the TST theory, which assumes that each crossing of the dividing surface corresponds to a true reactive event, in which the system passes from one state to another and then loses all memory of this transition before next event [173]. The TAD method further assumes the harmonic TST and thus is more approximate. In hyper-MD method, it is usually not easy to find a proper bias potential that modifies the potential energy without affecting the transition state regions. Examples of hyper-MD or TAD application to fracture simulations have not been encountered by the authors. However, a study by Wei [176] on strain-rate effects of nanotube fracture used the state transition theory concept which is similar to the TAD method.

5. Fracture of carbon nanotubes: An example

In this section, we provide detailed numerical results on a set of atomistic simulations of tensile loading over a range of strain rates at room temperature of carbon nanotubes leading to fracture. We consider a nanotube that has a pre-existing Stone–Wales defect (described later) at mid-section; we then compare the results with those from an initially defect-free nanotube. This numerical example demonstrates how the methodology works and describes the key features of AS, namely, potential model, initial condition, loading method, fracture criterion and extraction of information.

Carbon nanotubes (CNTs) have generated widespread interest since their discovery by Iijima in 1991 [177] due in part to their extraordinary mechanical properties. A substantial body of laboratory tests have suggested that CNTs have high elastic modulus (order of 1 TPa), high strength (order of 100 GPa), good ductility (up to 15% max strain), flexibility to bending and buckling and robustness under high pressure. Thus, CNTs hold great promise in a wide variety of innovative applications, such as in small scale electromechanical devices (gears, actuators, sensors, etc.), as nano-scale probes, as composite reinforcements, etc. Consequently, characterization of mechanical properties including the fracture process of nanotubes is an important element in the analysis and design of CNT-based materials and devices.

However, due to the small size of carbon nanotubes, laboratory experiments to measure their mechanical properties, and particularly to observe the evolution of their structures under loading, are difficult and potentially expensive at the current state of the art. This is particularly so when the effect of pre-existing defects at specified locations (possibly introduced to enhance electronic and/or mechanical performance of the CNT) needs to be investigated.

Nevertheless, elegant continuum approaches have also been used to study the mechanical properties of carbon nanotubes. In the quasi-continuum approach (discussed in Section 4.2) of Arroya [178] and Zhang et al. [179–181], the strain energy of the selected tube cell is calculated as the simple summation of all bond energy of all atomic bonds in the cell according to the Cauchy–Born rule. Assuming the nanotube is deformed uniformly before the onset of fracture, an analytical form of the summation can be easily formulated. Then mechanical properties (such as the elastic modulus) can be derived from the strain energy density formula. Zhang et al. [179,181] constructed the equilibrium equation, constitutive equation and boundary conditions for the nanotube; onset of fracture was treated as a bifurcation problem in the displacement increment field. Another approach developed by Li and Chou [139,182,183] is to model the atomic bonds as beams, so that the tube is modeled as a space frame. The stretching, bending and torsion stiffness of the 'beams' are determined by a set of interatomic potentials at zero strain. The nanotube is simplified to an elastic static problem, and its mechanical properties can be easily found through structural analysis, for example, the finite element method. These continuum approaches are computationally efficient compared with atomistic simulation, however, they both have limitations. They apply well to the *defect free* nanostructure; the quasi-continuum approach is especially preferred when the deformation is uniform, so that a closed form strain energy can be derived and the mechanical properties can be solved analytically.

And they are both intrinsically static (the kinetic energy of the atoms is not considered) making it more difficult to study dynamic properties.

Atomistic simulation, if used properly, has been proved to possess good combined performance in accuracy, economy, time and versatility. It is a very attractive tool that can complement laboratory experiments in studying the mechanical behavior and failure of carbon nanotubes. Therefore we choose simulation of the fracture process of a carbon nanotube with a pre-existing defect under tensile loading as a numerical example.

In this example, the structure subjected to simulation in this section is a (6, 6) armchair single-walled carbon nanotube with a Stone–Wales defect at mid-section. A single-walled nanotube (SWNT) is formed by rolling a sp^2 graphene sheet (composed of hexagons of carbon atoms) into a cylinder along a direction defined by the tube charility (m,n). SWNTs usually have diameters of ranging from less than 1 nm to tens of nm. Multi-walled nanotube (MWNT) contains several coaxial cylinders, each cylinder being a single-walled nanotube, with an interlayer distance of 0.34 nm. MWNTs usually have diameters of less then 100 nm, and length in micrometers [177,184–186]. The chirality, (m,n), of a carbon nanotube is defined in terms of a chiral vector $\mathbf{C}_n$ ($\mathbf{C}_n = m\mathbf{a}_1 + n\mathbf{a}_2$), which also determines the tube diameter d

$$d = a_0\sqrt{3(m^2 + n^2 + mn)}/\pi \tag{21}$$

The tube is built from wrapping a graphene sheet, in a direction defined by $\mathbf{C}_n$, superimposing its origin $(0,0)$ on its end (m,n). $\mathbf{a}_1$ and $\mathbf{a}_2$ are unit vectors, shown in Fig. 4. The parameter in Eq. (21), $a_0 = 1.42$ Å, is the carbon–carbon bond length in equilibrium. In this example, $m = n = 6$, which gives a so-called armchair chirality. A length of 20 hexagons is selected, so the tube is composed of 480 atoms, length, $l = 49.2$ Å, $d = 8.13$ Å.

The Stone–Wales (SW) defect is composed two pentagon–heptagon pairs, and can be formed by rotating an sp^2 bond by 90° (SW rotation) (Fig. 4). It is found that under certain conditions, SWNTs respond to the mechanical stimuli via the spontaneous formation of SW defect beyond an applied strain of around 5–6% [187]. The formation of SW defects is accompanied by elongation of the tube structure along the axis connecting the pentagons, and shrinking along the perpendicular direction. More interestingly, the SW defect can introduce successive SW rotations of different C–C bonds, which lead to gradual increase of tube length and shrinkage of tube diameter, resembling the necking phenomenon in tensile tests at macro scale. This process also gradually changes in chirality of the CNT, from armchair to zigzag direction. This whole response is plastic, with necking and growth of a "line defect", resembling the dislocation nucleation and moving in plastic deformation of crystal in many ways. Thus it is believed the SW defect has an important influence in the deformation of carbon nanotubes [188–190]. In this example, the SW defect is generated in the middle of the tube. The initial configuration of the tube is shown in Fig. 5(a).

The initial atomic velocities are randomly chosen according to a uniform distribution (between the limits −0.5 and 0.5) and then rescaled to match the initial temperature (300 K in this example, Eq. (16)). Since the

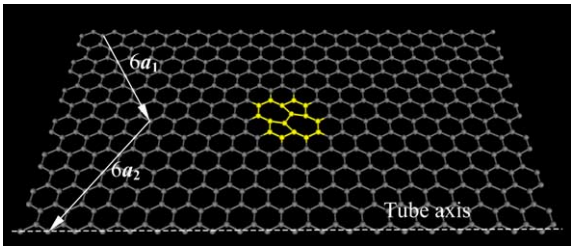

Fig. 4. Construction of a (6, 6) armchair SWNT with a Stone–Wales defect.

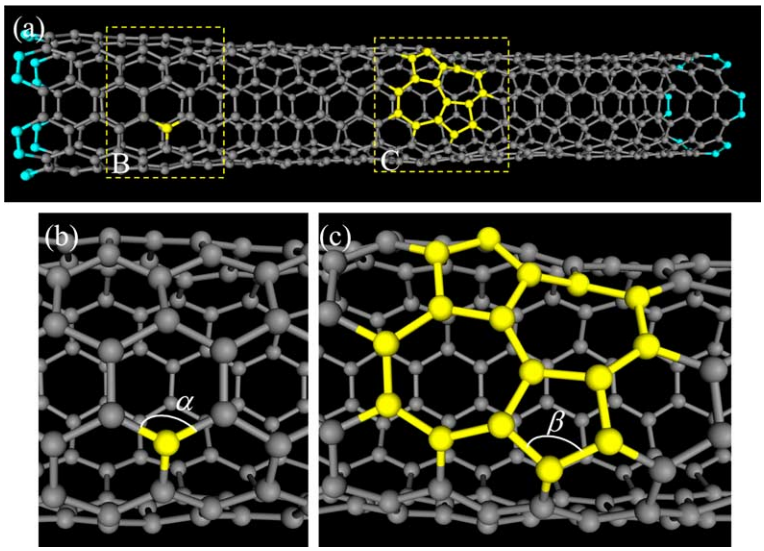

Fig. 5. Illustration of a (6,6) armchair single-walled carbon nanotube. (a) Full view of the SWNT; highlighted atoms in squares B, C show the angles to be monitored in the simulation; highlighted atoms at the ends are moved at constant speed during the simulations. (b) and (c) Squares B and C, enlarged, showing the angles monitored in the simulation.

temperature fluctuations in the subsequent simulations are within acceptable ranges, no temperature control is implemented.

The mechanical loading is applied through moving the atoms at both ends (highlighted at the ends of the tube in Fig. 5(a)) away from each other at a constant speed without relaxing until fracture occurs.

A modified Morse potential model for carbon [138] is applied. The potential energy has the form

$$E_i = E_{\text{stretch}} + E_{\text{angle}} = \sum_j E_{\text{stretch}}(i,j) + \sum_{jk} E_{\text{angle}}(i,j,k) \tag{22}$$

$$E_{\text{stretch}}(i,j) = D_e\{[1 - \mathrm{e}^{-\beta(r-r_0)}]^2 - 1\} \tag{23}$$

$$E_{\text{angle}}(i,j,k) = \frac{1}{2}k_\theta(\theta_{ijk} - \theta_0)^2[1 + k_{\text{sextic}}(\theta_{ijk} - \theta_0)^4] \tag{24}$$

This is the usual Morse potential except that the bond angle-bending energy has been added and the constants are slightly modified so that it corresponds with the Brenner potential [96] for strains below 10% [138]. E_{stretch} in Eq. (23) is the potential energy due to bond strength, r is the length of the bond; E_{angle} in Eq. (24) is the potential energy due to the bond angle-bonding, θ is the current angle of the adjacent bonds. The functions E_{stretch} and E_{angle} are illustrated in Fig. 6. The lowest energy points correspond, respectively, to the equilibrium distance of 1.42 Å and the equilibrium angle of 120° (2.094 rad). The potential model parameters are $r_0 = 1.39 \times 10^{-10}$ m, $D_e = 6.03105 \times 10^{-19}$ N m, $\beta = 2.625 \times 10^{10}$ m^{-1}, $\theta_0 = 2.094$ rad, $k_\theta = 0.9 \times 10^{-18}$ N m/rad^2, $k_{\text{sextic}} = 0.754$ rad^{-4}. For computational convenience, time, distance and quantities representing velocity, energy, etc. are reduced to non-dimensional numbers during the simulation; Table 2 shows the reduction of units. The Verlet algorithm (Eq. (3)) is applied for integration.

As discussed in Section 3.4, the bond-breaking criterion is an important issue in the simulation of fracture of solids. Most atomistic simulation studies adopt a distance-based criterion (r_f) for this and adopt the same cut-off distance (r_c) used in potential models as the numerical value for this critical interatomic

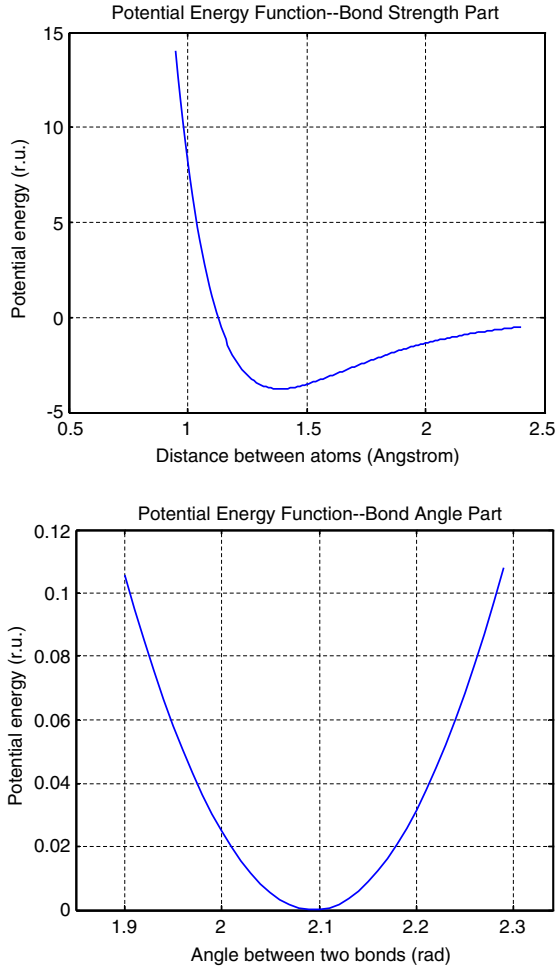

Fig. 6. Illustration of the bond strength part and bond angle part of the modified Morse potential.

separation. Nevertheless, it is important to remember that the potential cut-off distance is purely an artificial quantity introduced to facilitate computation and an inappropriately defined bond-breaking criterion may result in unrealistic results in fracture simulations. For example, the cut-off function in Brenner's bond order model is said to give rise to spurious forces and inaccurately large breaking strain [97,98,126]. Huhtala et al. [126] tested different cut-off distances for the bond order model, and found that although the spurious force remains, different cut-off distances (1.7 Å and 1.9 Å) apparently didn't change the critical bond-breaking force. The study by Xia [191] used a critical distance as 1.71 Å for carbon–carbon bond based on calculations of electron density around the breaking site. Dumitria et al. [192] used quantum mechanics simulation to study the bond-breaking bifurcation of carbon nanotubes by comparing energies of different breaking status at various strain levels. Their study showed that the carbon–carbon bond breaks between 1.7 and 1.9 Å. Therefore, based on the above discussion, we adopt $r_f = r_c = 1.77$ Å in this example.

In the following, results from a series of atomistic simulation of tensile loading of the (6, 6) armchair SWNT with an initial Stone–Wales defect at midsection are described. Time histories of potential energy, temperature, axial force and bond angle are extracted, and a series of snapshots detailing the progress of the fracture process is also provided. The Young's modulus (i.e., the initial slope of the force deformation

Table 2
Reduction of units for simulation

Quantity	Reduced units	Real units
Length	1	1×10^{-10} m
Energy	1	eV = 1.602×10^{-19} J
Mass	1	1.992×10^{-26} kg
Temperature	1	1.1609×10^{4} K
Time	1	3.526×10^{-14} s
Force	1	1.602×10^{-9} N
Pressure	1	160.2 GPa
Speed	1	2.836×10^{3} m/s
Potential model parameters Eqs. (23) and (24)		
	r.u.	Real units
r_0	1.39	1.39×10^{-10} m
D_e	3.7647	6.03105×10^{-19} N m
β	2.625	2.625×10^{10} m^{-1}
θ_0	2.094	2.094 rad
k_θ	5.6180	0.9×10^{-18} N m/rad^2
k_{sextic}	0.754	0.754 rad^{-4}

curve, suitably normalized), ultimate strength (i.e., the maximum force in the force time history divided by the nominal cross-sectional area), and ultimate strain (i.e., the engineering strain corresponding to the maximum force) of the tube are determined based on this information.

Fig. 7 shows the evolution of total energy, potential energy, temperature, displacements between the two ends of the tube and forces acting at one end of the tube, over 1.2 million time steps (one time step = 0.01 r.u. = 3.5×10^{-16} s). The loading rate, $v = 3.526 \times 10^{-4}$ r.u. which produces a displacement of 3.5×10^{-6} Å in one time step. As the displacement increases linearly with time, the force also increases in an approximate linear manner initially up to about the half-way point (time of 6000 r.u.) although there appears to be no clear yield point. The growth in force then decelerates up to the breaking point where an abrupt drop of force occurs. The axial force F_z is calculated by summing the forces acting on the atoms (boundary atoms highlighted in Fig. 5(a)) in axial direction at one end of the tube, and stress is calculated as $\sigma_{zz} = F_z/A$ in the following calculation. The cross-sectional area of the tube is taken to be 86.88 Å^2, based on the commonly adopted value of tube wall thickness of 0.34 nm [184] as stated above. For the purpose of comparison, the two alternate methods of calculating virial stress, Eqs. (18) and (19), are also applied, as shown in Fig. 8. The figure also shows the stress time history calculated using the current method (i.e., the sum of forces at one end of the tube, Eq. (20)). All three methods show practically the same long-term trend as expected for solids, but the force calculated from Eq. (18) has the least fluctuations since it is a volume averaged quantity.

The potential energy and the total energy show a nonlinear relation with displacement in Fig. 7. Assuming linear elastic behavior, the potential energy vs. displacement curve is expected to have a parabolic shape, and this fact can be used to derive the Young's modulus. The temperature can be seen to fluctuate around the preset temperature of 300 K throughout the loading process. However, at the initiation of fracture, the temperature increases abruptly and the potential energy drops.

For additional insight into the fracture process, time histories of two bond angles α and β are also plotted in Fig. 7 (the positions of these two angles are shown in Fig. 5(b) and (c)). The two angles have similar orientation but different locations. Angle α is the internal angle of an intact hexagon while angle β is an internal angle of a pentagon of the SW defect. As shown in Fig. 7, the two angles increase gradually from their equilibrium values (120° for angle α, and 108° for angle β) until the onset of fracture. At fracture,

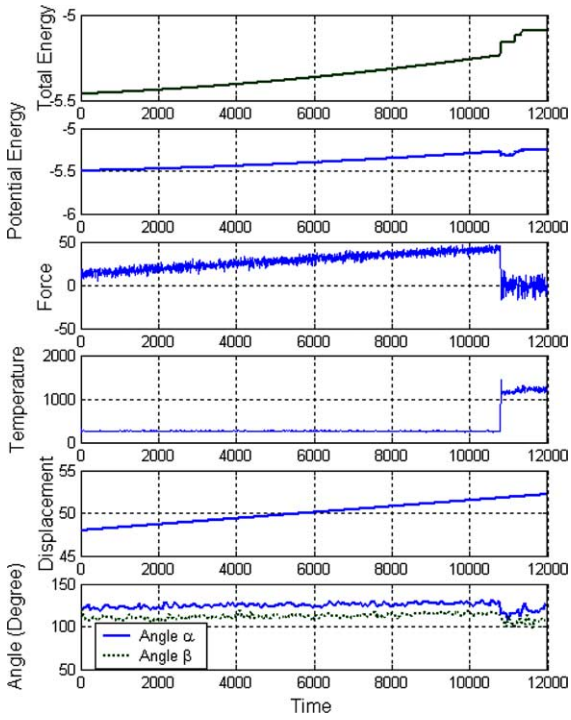

Fig. 7. Time history of a simulation of fracture process of a (6, 6) armchair SWNT with a pre-existing SW defect. All units are reduced (refer to Table 2) except for temperature (in Kelvin).

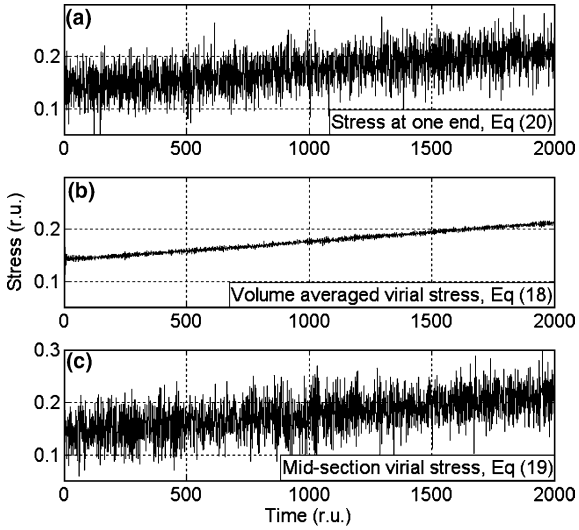

Fig. 8. Comparison among different methods for calculating stresses.

angle α drops abruptly and then fluctuates around its equilibrium value. Angle β drops too and fluctuates at an even lower value.

The detailed fracture process starting at around time 10786.6 r.u. and ending around time 10792 r.u. is shown in Fig. 9 while the corresponding force time history is magnified in Fig. 10. A total of 10 snapshots marked A–J have been identified and reproduced in Fig. 9, each of which corresponds to the breaking of one or more atomic bonds. The same 10 points have also been indicated in the time history of Fig. 10.

The Young's modulus and ultimate strength of the tube are now calculated from the force–displacement data plotted in Fig. 7. A second-order polynomial fit is applied to the stress–displacement curve (Fig. 8a) and the initial slope (multiplied with l/v) gives the Young's modulus, E. The resulting value is $E = 0.72$ TPa for the (6,6) armchair SWNT (at room temperature loaded at speed 3.526×10^{-4} r.u.). The ultimate strength is calculated based on the maximum value of the force time history (about 43 r.u. occurring around time 10 800 r.u.) acting on the tube ends. The computed value is thus $\sigma_u = 87.2$ GPa. The engineering definition of strain is adopted for this example (i.e., with respect to the original undeformed dimensions). The ultimate strain is found to be 7.3%.

The effect of loading speed on mechanical properties of the nanotube is investigated (Table 3 and Fig. 11): five loading speeds have been selected for this purpose ranging from 3.526×10^{-6} to 3.526×10^{-2} r.u. The ultimate strength is found to increase with increasing loading rate which agrees qualitatively with macroscopically observed behavior of engineering materials. The Young's modulus, on the other hand, appears much less sensitive to loading rate although there is an increasing trend. Interestingly, the ultimate strain displays a clearly increasing relation with loading rate which contradicts with that observed macroscopically for engineering materials. This particular behavior has significant potential for novel engineering applications. The results by Yakobson et al. [193] and Wei et al. [176] may be used here for comparison, showing that the breaking strain or yield strain increases as strain rate increases.

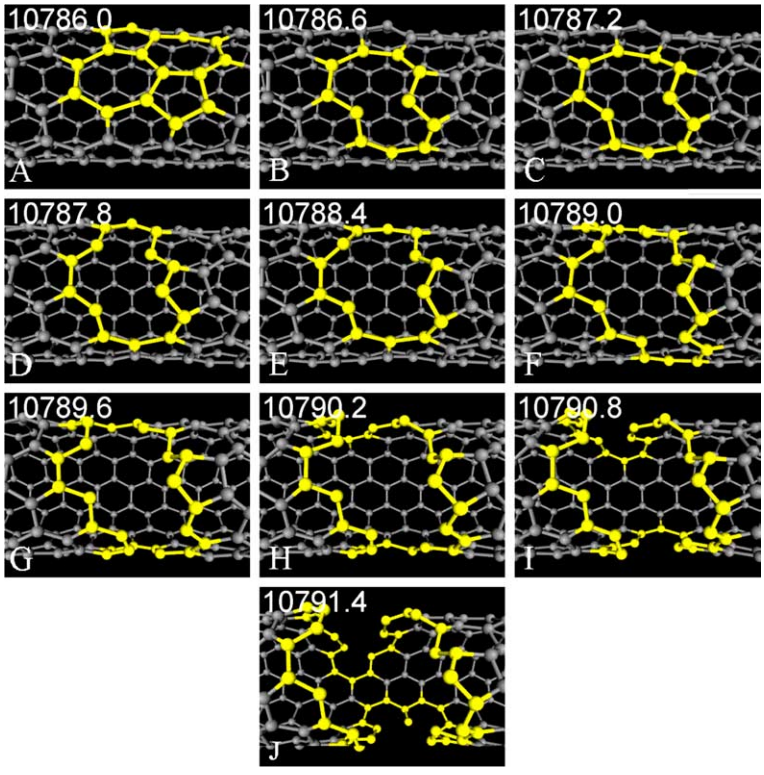

Fig. 9. Detailed fracture process; (A–J) snapshots taken as different time showing how bonds are broken and the crack develops.

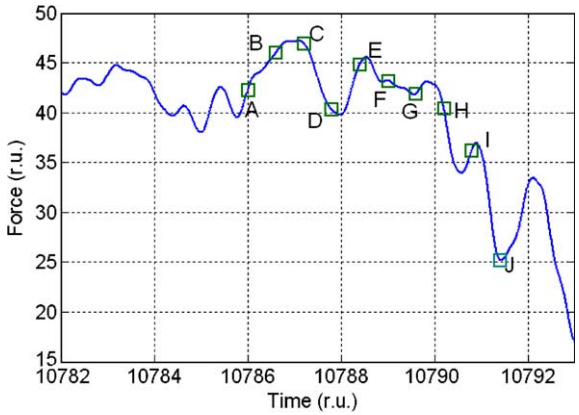

Fig. 10. Magnified force time history from the initiation to completion of fracture.

Table 3
Loading rate effects on mechanical properties of defect-free (6,6) SWNT and a (6,6) SWNT with a pre-existing Stone–Wales defect

	Initial elastic modulus (TPa)		Ultimate strength (GPa)		Ultimate strain (%)	
Speed (r.u.)	No defect	With defect	No defect	With defect	No defect	With defect
3.526×10^{-2}	0.818	0.845	95.0	81.7	9.89	6.34
3.526×10^{-3}	0.868	0.789	103	84.1	11.7	6.97
3.526×10^{-4}	0.829	0.722	106	87.2	12.3	7.34
3.526×10^{-5}	0.859	0.817	109	89.5	13.4	7.63
3.526×10^{-6}	0.865	0.837	110	95.9	14.3	9.50

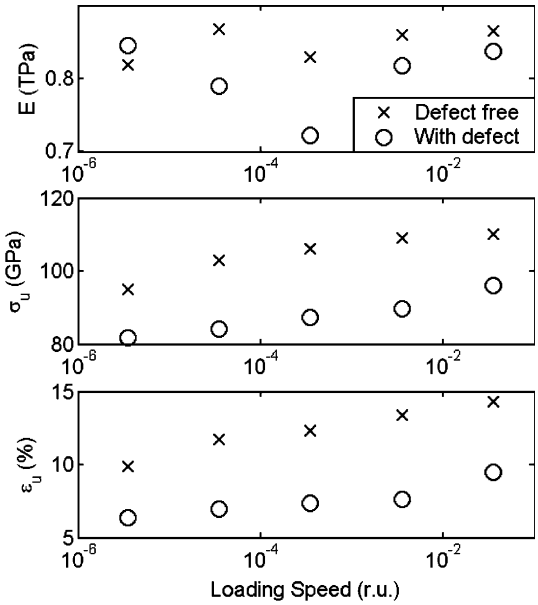

Fig. 11. Effects of loading speed on ultimate strength, elastic modulus and ultimate strain of the armchair SWNT (both with and without defect).

Table 4
A survey of Young's modulus of sing-walled carbon nanotubes

Ultimate strength (GPa)	Young's modulus (TPa)	Diameter (nm)	Length (nm)	Source, method/comment
NA	1.25–0.35/+0.45	1.0–1.5	23.4–36.8	[195], Thermal vibration experiment
NA	0.97–1.20	0.4–3.4	10	[196], AS using EAM potential. Modulus increases significantly with decreasing diameter and increase slightly with decreasing helicity
NA	0.8–1.22	0.8–2.0	NA	[197], Ab initio calculation. Modulus depends on chiralities
NA	0.50–0.82	0.6–1.4	Infinite[a]	[198], Ab initio calculation. Very little dependence on diameters and chiralities
$\geqslant 45 \pm 7$	NA	1.1–1.4	>4000	[199], AFM bending test on SWNT ropes. Maximum strain is measured as $(5.8 \pm 0.9)\%$, strength is calculated by assuming E is 1.25 TPa
NA	0.97	0.68–27	NA	[92], Empirical force constant model
NA	0.4–0.8	2.4–3.3	NA	[200], AS using Brenner's potential, tensile loading
NA	0.50	0.4–2.2	Infinite[a]	[201], AS using Brenner's potential, tensile loading
NA	0.98	1.3	14	[202], Tight binding
NA	1.2	3.1 ± 0.2	NA	[203], 3-point bending
NA	5.0	0.68	NA	[204], Tight binding calculation, wall thickness 0.7 Å
NA	4.70	NA	NA	[205], Local density approximation model, wall thickness 0.75 Å
65–93	NA	1.6	NA	[98], AS using modified Morse model, tensile loading
62.9	0.83–3.02	0.68	NA	[191], Atomistic simulation and ab initio calculation, w/o defects
40–50	1.0	0.4–2.2	6–1000	[176], Theoretical analysis based on AS. Modulus, yield strain and strength depend on loading rate. Yield strain depends on tube length
4.92	0.311	1.36	NA	[129], Tight-binding simulation, maximum strain 22%. Poisson ratio 0.287. Modulus slightly depends on diameters

[a] Simulating infinite long tube with periodic boundary condition.

Table 5
A survey of ultimate strength and Young's modulus of multi-walled carbon nanotubes

Ultimate strength (GPa)	Young's modulus (TPa)	Outer diameter (nm)	Length of tube (nm)	Method/comment
14.2 ± 8.0	1.28 ± 0.59	26–76	8.0	[206], Buckling stress is measured, which should be smaller than tensile strength. No dependence of Young's modulus on tube diameter
100–150	NA	21	Buckling: 18.3–68 Bending: 800	[207], Both bending and buckling tests are conducted. The strength is calculated from a maximum strain of 16% from bending
55	NA	8.4–16.6	46.2–436	[208], Critical buckling stress is measured
135–147	NA	19.6–56.2	Buckling length: 47–223.5	[209], Critical buckling stress is measured
11–63	0.27–0.95	13–33	6900–11 000	[210], Strength measured through direct stretching. Failure happens when the outermost layer is broken. No apparent dependence of tensile strength on the outer shell diameter. 12% strain at failure is measured
150	$0.91 \pm 20\%$	<10	About 500	[211], Strength measured through direct stretching
NA	0.6–1.1	10–20	NA	[212], Elastic modulus is measured through thermo-vibration method, higher modulus is found for thinner tubes
NA	0.1–1.6	12–30	1500–6250	[213], Elastic modulus is measured through resonant vibration, and found to decrease sharply with increasing diameter
NA	<0.12	30–250	About 2000	[214], Elastic modulus is measured through resonant vibration, and found to increase rapidly as diameter decreases
NA	0.67–1.1	$4.8–16.0 \pm 5\%$	240–420	[215], Elastic modulus is measured through beam deflection, and found no significant dependence on diameter

Finally, AS of tensile test of a *defect-free* (6,6) nanotube is also carried out at each of the above loading speeds. The final results are listed in Table 3 for comparison. One can readily find that the pre-existing SW defect significantly affects the mechanical properties. At all loading speeds, the tube with the defect (i) is significantly weaker than the defect free tube, (ii) breaks at a much smaller elongation compared to the defect free tube. As for the Young's modulus, the defect-free tube is found to be stiffer except at the smallest loading speed although the effect of the defect on stiffness is much less pronounced than in the case of the other two parameters.

The above mechanical properties can also be compared with available data obtained from laboratory and computational experiments conducted on carbon nanotubes of various sizes, chiralities, etc. Table 4 lists a collection of Young's modulus and ultimate strength data on SWNTs while, for the sake of completeness, Table 5 displays a similar collection for multi-walled nanotubes. It is clear that, while the results from this example agree with those in the existing literature, there is significant variation in the published data and it will be instructive to ascertain whether such variations arise from (i) atomic scale fluctuations including presence of defects, (ii) use of different loading methods, (iii) measurement errors, (iv) different methods of calculating cross-sectional areas and stresses, or a combination of these.

6. Summary and future needs

Broadly speaking, atomistic simulation is a powerful method to study fracture. Based on fundamental principles and simple ideas, it reveals the physical nature of fracture and can provide insight into the structural evolution at atomistic scale. This paper underlined the increasingly important role that AS has started to play in understanding the fracture process especially in aspects not served well by continuum mechanics. The development of AS for fracture over the past several decades was sketched. The essential steps in the methodology were detailed in terms of the potential model, initial conditions, loading method, temperature control and information extraction. Recent advances in the areas of ductile vs. brittle fracture, dynamic fracture and multi-scale simulation were detailed. Finally, a comprehensive example on the fracture simulation of a single wall carbon nanotube with a pre-existing Stone–Wales defect was described. Time histories of energy, force, bond angle and temperature were studied. The step by step progress of the fracture process was reproduced visually. Mechanical properties (Young's modulus, ultimate strength and ultimate strain) of the nanotube were determined and were compared with those of a defect-free nanotube; the effect of loading rate on these quantities was also investigated.

In spite of the increasing importance of AS in fracture research and the promise it holds for the future, this approach suffers from two significant shortcomings as outlined below.

(i) Relative inadequacy in description of the interaction between atoms compared with ab initio methods, especially when complex chemical effects are concerned. Currently classical atomistic simulations are applied to study materials composed of only one or a few types of atoms. Developing more accurate interatomic potential model and capable to deal with more types of atoms is a very important though challenging task. Nevertheless, improvements in physics and materials science are gradually eliminating this shortcoming. Ab initio calculations are used to develop more sophisticated potential models and to verify the results generated by atomistic simulations. Future potential models are expected to be more accurate in describing interatomic forces, more efficient in computation, more compatible with complex structures, components and environments.

(ii) Limitation of computation capacity on both time scale and space scale of simulations, when compared with continuum methods. Future work is expected to provide better integration methods to cross-scales, more effective technique for data processing and the information extraction after the computation. The work on the so-called multi-scale modeling method is far from complete. On the

time scale, the discrete time step Δt used in the simulations must be small enough to represent the movement of atoms correctly. However, the time scales of some characteristic phenomena (e.g. the emission, movement and entanglement of dislocations) are many orders larger. The computation cost to capture these effects satisfactorily is currently unacceptable. For the same reason, usually the loading speeds in atomistic simulations have to be very high in order to reduce the time of the whole loading process.

Improvements in small-scale imaging in recent years (neutron diffraction, X-ray diffraction, scanning tunneling electron microscopy, atomic force microscopy, etc.) will help provide better understanding of atomic structure and complement the results of atomistic simulation. More powerful computation techniques including parallel procession and data management will largely increase the capacity in both space and time scale of simulations. Better visualization techniques will provide vivid insight into rich diversity of the evolution of structure at small scales. It is hoped that accurate atomistic simulations of fracture at macro scales of space and time, subjected to realistic geometry, loading and environments, will be possible in the coming decades.

Acknowledgement

This work has been supported in part by a grant from the University of Delaware Research Foundation. The authors would also like to thank the reviewers for their helpful comments.

References

[1] Alder BJ, Wainwright TE. Molecular motions. Scient Am 1959;201(4):113.
[2] Allen MP, Tildesley DJ. Computer simulation of liquids. Oxford: Clarendon Press; 1989.
[3] Haile JM. Molecular dynamics simulation. New York: John Wiley & Sons, Inc.; 1997.
[4] Frenkel D, Smit B. Understanding molecular simulation, from algorithm to application. New York: Academic Press; 2002.
[5] Inglis CE. Stresses in a plate due to the presence of cracks and sharp corners. Trans Inst Naval Archit 1913;55:219–41.
[6] Griffith AA. The phenomena of rupture and flow in solids. Philos Trans R Soc London 1920;221:163–97.
[7] Irwin GR. Fracture dynamics. Fracturing of metals. Cleveland: A.S.f. Metals; 1948.
[8] Orowan E. Fracture and strength of solids. Reports on Progress in Physics XII; 1948. p. 185.
[9] Irwin GR. Analysis of stresses and strains near the end of a crack traversing a plate. J Appl Mech 1957;24:361–4.
[10] Westergaard HM. Bearing pressures and cracks. J Appl Mech 1939;6:49–53.
[11] Paris P, Erdogan F. A critical analysis of crack propagation laws. J Basic Engng 1963;85:528–34.
[12] Irwin GR. Plastic zone near a crack and fracture toughness. In: Sagamore Research Conference Proceedings; 1961.
[13] Dugdale DS. Yielding in steel sheets containing slits. J Mech Phys Solids 1960;8:100–8.
[14] Barenblatt GI. The mathematical theory of equilibrium cracks in brittle fracture. Adv Appl Mech 1962;7:55–129.
[15] Wells, AA. Unstable crack propagation in metals: cleavage and fast fracture. In: Proceedings of the Crack Propagation Symposium, Cranfield, UK; 1961.
[16] Rice JR. A path independent integral and the approximate analysis of strain concentrations by notches and cracks. J Appl Mech 1968;35:379–86.
[17] Hutchinson JW. Singular behavior at the end of a tensile crack in a hardening material. J Mech Phys Solids 1968;16: 13–31.
[18] Rice JR, Rosengren GF. Plane strain deformation near a crack tip in a power-law hardening material. J Mech Phys Solids 1968;16:1–12.
[19] Sanders JL. On the Griffith–Irwin fracture theory. J Appl Mech 1960;27:352–3.
[20] Eshelby JD. Energy relations and the energy–momentum tensor in continuum mechanics. In: Kanninen MF et al., editors. Inelastic behavior of solids. New York: McGraw-Hill; 1969. p. 77–115.
[21] Cherepanov GP. On crack propagation in solids. Int J Solids Struct 1969;5:863–71.
[22] Begley JA, Landes JD. The *J*-integral as a fracture criterion. ASTM STP 514. Philadelphia: American Society for Testing and Materials; 1972. p. 1–20.

[23] Shih CF, Hutchinson JW. Fully plastic solutions and large-scale yielding estimates for plane stress crack problems. J Engng Mater Technol 1976;98:289–95.
[24] Shih CF. Relationship between the *J*-integral and the crack opening displacement for stationary and extending cracks. J Mech Phys Solids 1981;29:305–26.
[25] Mott NF. Fracture of metals: theoretical considerations. Engngineering 1948;165:16–8.
[26] Dulaney EN, Brace WF. Velocity behavior of a growing crack. J Appl Phys 1960;31:2233–6.
[27] Berry JP. Some kinetic considerations of the Griffith criterion for fracture. J Mech Phys Solids 1960;8:194–216.
[28] Roberts DK, Wells AA. The velocity of brittle fracture. Engineering 1954;178:820–1.
[29] Yoffe EH. The moving Griffith crack. Philos Mag 1951;42:739–50.
[30] Broberg KB. The propagation of a brittle crack. Arkiv Fysik 1960;18:159–92.
[31] Atkinson C, Eshelby JD. The flow of energy into the tip of a moving crack. Int J Fract Mech 1968;4:3–8.
[32] Freund LB. Crack propagation in an elastic solid subjected to general loading—I. Constant rate of extension. J Mech Phys Solids 1972;20:129–40.
[33] Freund LB. Crack propagation in an elastic solid subjected to general loading—III. Stress wave loading. J Mech Phys Solids 1973;21:47–61.
[34] Freund LB. Crack propagation in an elastic solid subjected to general loading—II. Non-uniform rate of extension. J Mech Phys Solids 1972;20:141–52.
[35] Nilsson F. A note on the stress singularity at a non-uniformly moving crack tip. J Elast 1974;4:73–5.
[36] Schardin H. Velocity effects in fracture. In: Fracture. Cambridge, MA: MIT Press; 1959. p. 297–330.
[37] Hudson G, Grennfield M. Speed of propagation of brittle cracks in steel. J Appl Phys 1947;18:405–8.
[38] Wells AA, Post D. The dynamic stress distribution surrounding a running crack—a photoelastic analysis. Proc Soc Exper Stress Anal 1958;16:69–92.
[39] Carlsson AJ. On the mechanism of brittle fracture propagation. Trans R Inst Technol (Sweden) 1963;205:2–38.
[40] Kanninen MF, Popelar CH. Advanced fracture mechanics. Oxford University Press; 1985.
[41] Anderson TL. Fracture mechanics: fundamentals and applications. 2nd ed. Boca Raton, FL: CRC Press; 1995.
[42] Broek D. Elementary engineering fracture mechanics. 4th ed. Berlin: Kluwer Academic; 1991.
[43] ASME, Boilers And Pressure Vessels Code, New York: American Society of Mechanical Engineers; 2001.
[44] BSI, Gas cylinders. Refillable seamless steel. Performance tests. Fracture performance tests. Monotonic burst tests, Chichester: British Standards Publishing Limited (BSPL); 2002.
[45] AASHTO, Manual for condition evaluation and load and resistance factor rating (LRFR) of highway bridge., Washington, DC: American Association of State Highway and Transportation Officials; 2003.
[46] API, API-579 Fitness For Service. Washington, DC: American Petroleum Institute; 2000.
[47] ASTM, E1820-01 Standard Test Method for Measurement of Fracture Toughness. West Conshohocken: American Society for Testing and Materials; 2001.
[48] Hori M, Nemat-Nasser S. On two micromechanics theories for determining micro–macro relations in heterogeneous solids. Mech Mater 1999;31(10):667–82.
[49] Sobczyk K, Kirkner DJ. Stochastic modeling of microstructures. Boston: Birkhäuser; 2001.
[50] Torquato S. Random heterogeneous materials: microstructure and macroscopic properties. New York: Springer; 2002.
[51] Thomson R et al. Lattice trapping of fracture cracks. J Appl Phys 1971;42(8):3154–60.
[52] Kohlhoff S, Gumbsch P, et al. Crack-propagation in BCC crystals studied with a combined finite-element and atomistic model. Philos Mag A 1991;64(4):851–78.
[53] Riedle J et al. Cleavage anisotropy in tungsten single crystals. Phys Rev Lett 1996;76(19):3594–7.
[54] Perez R, Gumbsch P. An ab initio study of the cleavage anisotropy in silicon. Acta Mater 2000;48:4517–30.
[55] Perez R, Gumbsch P. Directional anisotropy in the cleavage fracture of silicon. Phys Rev Lett 2000;84(23):5347–50.
[56] Michot G. Crystal properties and preparation, vol. 17–18; 1988.
[57] George A, Michot G. Dislocation loops at crack tips: nucleation and growth—an experimental study in silicon. Mater Sci Engng A 1993;164(1–2):118–34.
[58] Beltz GE, Lipkin DM. A dislocation model for the directional anisotropy of grain-boundary fracture. MRS Bull 2000;25(5):21.
[59] Yokobori T. The unfied philosophies in fracture. In: Cherepanov GP, editor. Fracture: a topical encyclopedia of current knowledge. Malabar, FL: Krieger Publishing Company; 1998.
[60] Rice JR, Thomson R. Ductile versus brittle behavior of crystals. Philos Mag 1974;29(1):73–97.
[61] Hirsch PB, Roberts SG, Samuels J. The brittle–ductile transition in silicon. II. Interpretation. Proc R Soc London Ser A 1989; 421(1860):25–53.
[62] Rice JR. Dislocation nucleation from a crack tip: an analysis based on the peierls concept. J Mech Phys Solids 1992;40(2): 239–71.
[63] van der Giessen E, Needleman. Discrete dislocation plasticity: a simple planar model. Model Simulat Mater Sci Engng 1995; 3(5):689.

[64] Hutchinson HB, Dickey JE, Thomson R. Dislocation energies in NaCl. Phys Rev 1955;100:1117.
[65] Doyama M, Cotterill MJ. Energy and atomic configurations of complete and dissociated dislocations. II. Screw dislocation in an fcc metal. Phys Rev 1966;150:448–55.
[66] Chang R. An atomic study of fracture. Int J Fract Mech 1970;6(2):111.
[67] Kanninen MF, Gehlen PC. Atomic simulation of crack extension in bcc iron. Int J Fract Mech 1971;7:471–4.
[68] Sinclair JE. Improved atomistic model of a bcc dislocation core. J Appl Phys 1971;42(13):5321.
[69] Sinclair JE. The influence of the interatomic force law and of kinks on the propagation of brittle cracks. Philos Mag 1975;31(3):647–71.
[70] Harris J. Simplified method for calculating the energy of weakly interacting fragments. Phys Rev B 1985;31(4):1770–9.
[71] Bernstein N, Kaxiras E. Nonorthogonal tight-binding Hamiltonians for defects and interfaces in silicon. Phys Rev B 1997; 56(16):10488–96.
[72] Car R, Parrinello M. Unified approach for molecular-dynamics and density-functional theory. Phys Rev Lett 1985;55(22): 2471–4.
[73] Marx D, Parrinello M. Ab initio path integral molecular dynamics: basic ideas. J Chem Phys 1996;104(11):4077–82.
[74] Raabe D. Computational material science, the simulation of materials microstructures and properties. New York: Academic Press; 1998.
[75] Lennard-Jones JE. On the determination of molecular fields. II. From the equation of state of a gas. Proc R Soc London Ser A 1924;106(738):463–77.
[76] Morse PM. Diatomic molecules according to the wave mechanics. II. Vibrational levels. Phys Rev 1929;34(57).
[77] Girifalco LA, Weizer VG. Application of the Morse potential function to cubic metals. Phys Rev 1959;114:687–90.
[78] Lincoln RC, Koliwad KM, Ghate PB. Morse-potential evaluation of second- and third-order elastic constants of some cubic metals. Phys Rev 1967;157(3):463.
[79] Roy D, Manna A, et al. Application of Morse potential function in ordered Cu3Au alloy. 2. Thermal-expansion and equation of state. J Phys F-Metal Phys 1974;4(12):2145–51.
[80] Weizer VG, Girifalco LA. Vacancy–vacancy interaction in copper. Phys Rev 1960;120(3):837–9.
[81] Johnson RA. Interstitials and vacancies in alpha iron. Phys Rev 1964;134:A1329–36.
[82] Johnson RA. Calculations of small vacancy and interstitial clusters for an fcc lattice. Phys Rev 1966;152:629–34.
[83] Abraham FF, Walkup R, et al. Simulating materials failure by using up to one billion atoms and the world's fastest computer: brittle fracture. Proc Natl Acad Sci The United States of America 2002;99(9):5777–82.
[84] Taylor R. A critique of the practice of fitting pair potentials to experiment data. In: Lee JK, editor. Interatomic potentials and crystalline defects. Warrendale, PA: Metallurgical Society of AIME; 1980.
[85] Finnis MW, Sinclair JE. A simple empirical N-body model for transition metals. Philos Mag A 1984;50(1):45–55.
[86] Rasolt M, Taylor R. Charge densities and interionic potentials in simple metals: nonlinear effects. I. Phys Rev B 1975;11: 2717–25.
[87] Dagens L, Rasolt M, Taylor R. Charge densities and interionic potentials in simple metals: nonlinear effects. II. Phys Rev B 1975; 11:2726–34.
[88] Daw MS, Baskes MI. Semiempirical, quantum mechanical calculation of hydrogen embrittlement in metals. Phys Rev Lett 1983;50(17):1285–8.
[89] Daw MS, Baskes MI. Embedded-atom method: derivation and application to impurities, surfaces, and other defects in metals. Phys Rev B 1984;29(12):6443–53.
[90] Foiles SM, Baskes MI, Daw MS. Embedded-atom-method functions for the fcc metals Cu, Ag, Au, Ni, Pd, Pt, and their alloys. Phys Rev B 1986;33:7983–91.
[91] Sutton AP, Chen J. Long-range finnis Sinclair potentials. Philos Mag Lett 1990;61(3):139–46.
[92] Lu H, Rafii-Tabar H, Cross M. Molecular dynamics simulation of fractures using an N-body potential. Philos Mag Lett 1997; 75(5):237–44.
[93] Stillinger FH, Weber TA. Computer simulation of local order in condensed phases of silicon. Phys Rev B 1985;31(8):5262–70.
[94] Tersoff J. New empirical-approach for the structure and energy of covalent systems. Phys Rev B 1988;37(12):6991–7000.
[95] Tersoff J. Carbon defects and defect reactions in silicon. Phys Rev Lett 1990;64(15):1757–60.
[96] Brenner DW. Empirical potential for hydrocarbons for use in simulating the chemical vapor deposition of diamond films. Phys Rev B 1990;42(15):9458–71.
[97] Troya D, Mielke SL, Schatz GC. Carbon nanotube fracture—differences between quantum mechanical mechanisms and those of empirical potentials. Chem Phys Lett 2003;382(1–2):133–41.
[98] Belytschko T et al. Atomistic simulations of nanotube fracture. Phys Rev B (Cond Matter Mater Phys) 2002;65(23):235430–8.
[99] Bazant MZ, Kaxiras E. Modelling of covalent bonding in solids by inversion of cohesive energy curves. Phys Rev Lett 1996; 77(21):4370–3.
[100] Bazant MZ, Kaxiras E. Environment-dependent interatomic potential for bulk silicon. Phys Rev B 1997;56(14):8542–52.
[101] Justo JF, Bazant MZ, et al. Interatomic potential for silicon defects and disordered phases. Phys Rev B 1998;58(5):2539–50.

[102] Marks NA. Generalizing the environment-dependent interaction potential for carbon. Phys Rev B 2002;63:035401.
[103] Maki-Jaskari M, Kaski K, Kuronen A. Simulations of crack initiation in silicon. Computat Mater Sci 2000;17:336–42.
[104] Sih GC, Liebowitz H. In: Liebowitz H, editor. Fracture: an advanced treatise. New York, London: Academic Press; 1968. p. 125.
[105] Ashurst WT, Hoover WG. Microscopic fracture studies in the two-dimensional triangular lattice. Phys Rev B 1976;14:1465–73.
[106] de Celis B, Argon AS, Yip S. Molecular dynamics simulation of crack tip processes in alpha-iron and copper. J Appl Phys 1983;54(9):4864–78.
[107] Hoagland RG, Daw MS, Hirth JP. J Mater Res 1991;6:2565.
[108] Cheung KS, Yip S. Brittle–ductile transition in intrinsic fracture behavior of crystals. Phys Rev Lett 1990;65:2804–7.
[109] Cleri F et al. Atomic-scale mechanism of crack-tip plasticity: dislocation nucleation and crack-tip shielding. Phys Rev Lett 1997;79(7):1309–12.
[110] Cleri F et al. Atomistic simulations of materials fracture and the link between atomic and continuum length scales. J Am Ceram Soc 1998;81(3):501–16.
[111] Guo YF et al. Atomistic simulation of crack cleavage and blunting in bcc-Fe. Mater Sci Engng A 2003;349(1–2):29–35.
[112] Nakano A et al. Scalable molecular-dynamics, visualization, and data-management algorithms for materials simulations. Comput Sci Engng 2001;1(5):39–47.
[113] Abraham FF, Walkup R, et al. Simulating materials failure by using up to one billion atoms and the world's fastest computer: work-hardening. Proc Natl Acad Sci The United States of America 2002;99(9):5783–7.
[114] Nose S. A molecular dynamics method for simulations in the canonical ensemble. Mol Phys 1984;52:255.
[115] Hoover WG. Canonical dynamics: equilibrium phase-space distributions. Phys Rev A 1985;31(3):1695.
[116] Martyna GJ, Klein ML, Tuckerman M. Nose–Hoover chains: the canonical ensemble via continuous dynamics. J Chem Phys 1992;97(4):2635.
[117] Branka AC. Nose–Hoover chain method for non-equilibrium molecular dynamic simulation. Phys Rev E 2000;61(5):4769.
[118] Branka AC, Kowalik M, Wojciechowski KW. Generalization of the Nose–Hoover approach. J Chem Phys 2003;119(4):1929.
[119] Anderson HC. Molecular dynamics at constant pressure and/or temperature. J Chem Phys 1980;72:2384–93.
[120] Liu Y, Tuckerman ME. Generalized Gaussian moment thermostatting: a new continuous dynamical approach to the canonical ensemble. J Chem Phys 2000;112(4):1685.
[121] Holian BL, Voter AF, Ravelo R. Thermostatted molecular dynamics: how to avoid the Toda demon hidden in Nose–Hoover dynamics. Phys Rev E 1995;52(3):2338.
[122] Gumbsch P. Brittle fracture processes modeled on the atomic scale. Zeit Metall 1996;87(5):341–8.
[123] Machova A, Kroupa F. Atomistic modelling of contribution of dislocations to crack opening displacements. Mater Sci Engng A 1997;234–236:185–8.
[124] Marder M. Molecular dynamics of cracks. Comput Sci Engng 1999;1(5):48–55.
[125] Swadener JG, Baskes MI, Nastasi M. Molecular dynamics simulation of brittle fracture in silicon. Phys Rev Lett 2002;89:085503.
[126] Huhtala M et al. Improved mechanical load transfer between shells of multiwalled carbon nanotubes. Phys Rev B 2004; 70(4).
[127] Zhou SJ et al. Large-scale molecular dynamic simulations of three-dimensional ductile fracture. Phys Rev Lett 1997;78(3):479.
[128] Jin Y, Yuan FG. Simulation of elastic properties of single-walled carbon nanotubes. Compos Sci Technol 2003;63(11):1507–15.
[129] Dereli G, Ozdogan C. Structural stability and energetics of single-walled carbon nanotubes under uniaxial strain. Phys Rev B 2003;67(3):035416.
[130] Clausius R. On a mechanical theory applicable to heat. Philos Mag 1870;40:122–7.
[131] Lutsko JF. Stress and elastic constants in anisotropic solids: molecular dynamics techniques. J Appl Phys 1988;64(3):1152–4.
[132] Tsai DH. The virial theorem and stress calculation in molecular dynamics. J Chem Phys 1979;70:1375–82.
[133] Cheung KS, Yip S. Atomic-level stress in an inhomogeneous system. J Appl Phys 1991;70(10):5688–90.
[134] Cormier J, Rickman JM, Delph TJ. Stress calculation in atomistic simulations of perfect and imperfect solids. J Appl Phys 2001;89(1):99–104.
[135] Zhou LG, Shi SQ. Molecular dynamic simulations on tensile mechanical properties of single-walled carbon nanotubes with and without hydrogen storage. Computat Mater Sci 2002;23:166–74.
[136] Zhou M. A new look at the atomic level virial stress: on continuum-molecular system equivalence. Proc R Soc London Ser A-Math Phys Engng Sci 2003;459(2037):2347–92.
[137] Lier GV et al. Ab initio study of the elastic properties of single-walled carbon nanotubes and graphene. Chem Phys Lett 1999;326(1–2):181–5.
[138] Belytschko T et al. Atomistic simulations of nanotube fracture. Phys Rev B 2002;65:235430.
[139] Li CY, Chou TW. Elastic moduli of multi-walled carbon nanotubes and the effect of van der Waals forces. Compos Sci Technol 2003;63(11):1517–24.
[140] Nakano A, Kalia RK, Vashishta P. Scalable molecular-dynamics, visualization, and data-management algorithms for materials simulations. Comput Sci Engng 1999;1(5):39–47.

[141] Ludwig M, Gumbsch P. Cleavage fracture and crack tip dislocation emission in B2 NiAl: an atomistic study. Acta Mater 1998; 46(9):3135–43.
[142] Riemelmoser FO. Dislocation modeling of fatigue cracks: an overview. Mater Trans JIM 2001;42(1):2–13.
[143] Schoeck G. The emission of dislocation from crack tips, A critical review. Mater Sci Engng A 2003;356:93–101.
[144] Farkas D. Atomistic studies of intrinsic crack-tip plasticity. MRS Bull 2000;25(5):35.
[145] Zhou SJ, Carlsson AE, Thomson R. Dislocation nucleation and crack stability: lattice Green's-function treatment of cracks in a model hexagonal lattice. Phys Rev B 1993;47:7710.
[146] Zhou SJ, Carlsson AE, Thomson R. Crack blunting effects on dislocation emission from cracks. Phys Rev Lett 1994; 72(6–7):852–5.
[147] Knap J, Sieradzki K. Crack tip dislocation nucleation in FCC solids. Phys Rev Lett 1999;82:1700–3.
[148] Farkas D. Fracture toughness from atomistic simulations: brittleness induced by emission of sessile dislocations. Scr Mater 1998;39(4–5):533–6.
[149] Khantha M, Pope DP, Vitek V. The brittle-to-ductile transition. 1. A cooperative dislocation generation instability. Scr Metal Mater 1994;31(10):1349–54.
[150] Khantha M. The brittle-to-ductile transition. 2. Dislocation dynamics and the strain-rate dependence of the transition-temperature. Scr Metal Mater 1994;31(10):1355–60.
[151] Rosakis AJ, Samudrala O, Coker D. Cracks faster than the shear wave speed. Science 1999;284:1337–40.
[152] Abraham FF et al. Instability dynamics of fracture: a computer simulation investigation. Phys Rev Lett 1994;73:272–5.
[153] Cui FZ et al. Atomistic simulation of radiation damage to carbon nanotube. Phys Lett 2002;295:55–9.
[154] Hu Z et al. Hydrogen embrittlement of a single crystal of iron on a nanometre scale at a crack tip by molecular dynamics. Model Simulat Mater Sci Engng 1999;7(4):541–51.
[155] Machova A. Brittle–ductile behavior in bcc iron containing copper nano-particles. Mater Sci Engng A 2001;A319–321:574–7.
[156] Trachenko KO, Dove MT, Salje EKH. Atomistic modelling of radiation damage in zircon. J Phys Cond Matter 2001;13(9):1947.
[157] Vashishta P et al. Multimillion atom simulation of materials on parallel computers—nanopixel, interfacial fracture, nanoindentation, and oxidation. Appl Surf Sci 2001;182:258–64.
[158] Heffelfinger GS. Parallel atomistic simulations. Comput Phys Commun 2000;128:219–37.
[159] Refson K. Moldy: a protable molecular dynamics simulation program for serial and parallel computers. Comput Phys Commun 2000;126:310–29.
[160] Nelson MT et al. NAMD: a parallel, object oriented molecular dynamics program. Int J Supercomput Applic High Perform Comput 1996;10(4):251–68.
[161] Deymier PA, Vasseur JO. Concurrent multiscale model of an atomic crystal coupled with elastic continua. Phys Rev B 2002;66(13):134106.
[162] Nieminen NM. From atomistic simulation towards multiscale modeling of materials. J Phys Cond Matter 2002;14:2859–76.
[163] Kröner E. On the physical reality of torque stresses in continuum mechanics. Int J Engng Sci 1963;1:261.
[164] Curtin WA, Miller R. Atomistic/continuum coupling in computational materials science. Model Simulat Mater Sci Engng 2003; 11:R33–86.
[165] Tadmor EB, Phillips R, Ortiz M. Mixed atomistic and continuum models of deformation in solids. Langmuir 1996;12:4529–34.
[166] Shenoy VB et al. An adaptive_nite element approach to atomic-scale mechanics∗the quasicontinuum method. J Mech Phys Solids 1999;47:500–31.
[167] Shenoy VB et al. An adaptive methodology for atomic scale mechanics: the quasicontinuum method. J Mech Phys Solids 1999;47:611–42.
[168] Knap J, Ortiz M. An analysis of the quasicontinuum method. J Mech Phys Solids 2001;49:1899–923.
[169] Miller R, Tadmor EB. The quasicontinuum method: overview, applications and current directions. J Comput-Aided Mater Des 2002;9:203–39.
[170] Abraham FF, Broughton JQ. Spanning the length scales in dynamic simulation. Comput Phys 1998;12(6):538–46.
[171] Shilkrot LE, Miller RE, Curtin WA. Coupled atomistic and discrete dislocation plasticity. Phys Rev Lett 2002;89(2):025501.
[172] Voter AF. Hyperdynamics: accelerated molecular dynamics of infrequent events. Phys Rev Lett 1997;78(20):3908–11.
[173] Voter AF. A method for accelerating the molecular dynamics simulation of infrequent events. J Chem Phys 1997;106(11): 4665–77.
[174] Sorensen MR, Voter AF. Temperature-accelerated dynamics for simulation of infrequent events. J Chem Phys 2000;112(21): 9599–606.
[175] Hanggi P, Talkner P, Borkovec M. Reaction-rate theory—50 years after Kramers. Rev Modern Phys 1990;2(2):251–341.
[176] Wei C, Cho K, Srivastava D. Tensile strength of carbon nanotubes under realistic temperature and strain rate. Phys Rev B 2003;67:115407.
[177] Iijima S. Helical microtubules of graphitic carbon. Nature 1991;354:56.
[178] Arroyo M, Belytschko T. Nonlinear mechanical response and rippling of thick multiwalled carbon nanotubes. Phys Rev Lett 2003;91(21):215505.

[179] Zhang P et al. Fracture nucleation in single-wall carbon nanotubes under tension: a continuum analysis incorporating interatomic potentials. J Appl Mech-Trans ASME 2002;69(4):454–8.
[180] Zhang P et al. The elastic modulus of single-wall carbon nanotubes: a continuum analysis incorporating interatomic potentials. Int J Solids Structs 2002;39(13–14):3893–906.
[181] Zhang P et al. An atomistic-based continuum theory for carbon nanotubes: analysis of fracture nucleation. J Mech Phys Solids 2004;52(5):977–98.
[182] Li C, Guo WL. Continuum mechanics simulation of post-buckling of single-walled nanotubes. Int J Nonlinear Sci Numer Simulat 2003;4(4):387–93.
[183] Li CY, Chou TW. Modeling of elastic buckling of carbon nanotubes by molecular structural mechanics approach. Mech Mater 2004;36(11):1047–55.
[184] Iijima S, Ichihashi T, Ando Y. Pentagons, heptagons and negative curvature in graphite microtubule growth. Nature 1992; 356(776).
[185] Terrones M. Science and technology of the twenty-first century: synthesis, properties, and applications of carbon nanotubes. Annu Rev Mater Res 2003;33:419–501.
[186] Dresselhaus MS, Dresselhaus G, Avouris P. Carbon nanotubes: synthesis, structure, properties, and applications. Berlin, New York: Springer; 2001.
[187] Nardelli MB, Yakobson BI, Bernholc J. Mechanism of strain release in carbon nanotube. Phys Rev B 1998;57(8):R4277.
[188] Chandra N, Namilae S, Shet C. Local elastic properties of carbon nanotubes in the presence of Stone–Wales defects. Phys Rev B 2004;69(9):094101.
[189] Liew KM, He XQ, Wong CH. On the study of elastic and plastic properties of multi-walled carbon nanotubes under axial tension using molecular dynamics simulation. Acta Mater 2004;52(9):2521–7.
[190] Liew KM et al. Nanomechanics of single and multiwalled carbon nanotubes. Phys Rev B 2004;69(11).
[191] Xia YY et al. Tensile strength of single-walled carbon nanotubes with defects under hydrostatic pressure. Phys Rev B 2002; 65(15).
[192] Dumitrica T, Belytschko T, Yakobson BI. Bond-breaking bifurcation states in carbon nanotube fracture. J Chem Phys 2003;118(21):9485–8.
[193] Yakobson BI et al. High strain rate fracture and C-chain unraveling in carbon nanotubes. Computat Mater Sci 1997;8(4): 283–365.
[194] Kittel C. Introduction to solid state physics. John Wiley & Sons, Inc.; 1996.
[195] Krishnan A et al. Young's modulus of single-walled nanotubes. Phys Rev B 1998;58(20):14013–9.
[196] Yao N, Lordi V. Young's modulus of single-walled carbon nanotubes. J Appl Phys 1998;84(4):1939.
[197] Hernandez E, Goze C, Bernier P. Elastic properties of C and $B_xC_yN_z$ composite nanotubes. Phys Rev Lett 1998;80(20):4502–5.
[198] Sanchez-Portal D et al. Ab initio structural, elastic, and vibrational properties of carbon nanotubes. Phys Rev B 1999;59(19): 12678–88.
[199] Walters DA et al. Elastic strain of freely suspended single-wall carbon nanotube ropes. J Appl Phys 1999;74(25):3803–5.
[200] Cornwell CF, Wille LT. Simulations of the elastic response of single-walled carbon nanotubes. Computat Mater Sci 1998; 10(1–4):42–5.
[201] Halicioglu T. Stress calculations for carbon nanotubes. Thin Solid Films 1998;312(1–2):11–4.
[202] Ozaki T, Iwasa Y, Mitani T. Stiffness of single-walled carbon nanotubes under large strain. Phys Rev Lett 2000;84(8):1712–5.
[203] Tombler TW et al. Reversible electromechanical characteristics of carbon nanotubes under local-probe manipulation. Nature 2000;405(6788):769–72.
[204] Zhou X, Zhou JJ, Ou-Yang ZC. Strain energy and Young's modulus of single-wall carbon nanotubes calculated from electronic energy-band theory. Phys Rev B 2000;62(20):13692–6.
[205] Tu Z-c, Ou-Yang Z-c. Single-walled and multiwalled carbon nanotubes viewed as elastic tubes with the effective Young's moduli dependent on layer number. Phys Rev B Cond Matter Mater Phys 2002;65(23):233407–14.
[206] Wong EW, Sheehan PE, Lieber CM. Nanobeam mechanics: elasticity, strength, and toughness of nanorods and nanotubes. Science 1997;277(5334):1971–5.
[207] Falvo MR et al. Bending and buckling of carbon nanotubes under large strain. Nature 1997;389:582.
[208] Wagner HD et al. Stress-induced fragmentation of multiwall carbon nanotubes in a polymer matrix. Appl Phys Lett 1998; 72(2):188.
[209] Lourie O, Cox DM, Wagner HD. Buckling and collapse of embedded carbon nanotubes. Phys Rev Lett 1998;81(8):1638.
[210] Yu MF, Lourie O, Dyer MJ. Strength and breaking mechanism of multiwalled carbon nanotubes under tensile load. Science 2000;287(5453):637–40.
[211] Demczyk BG et al. Direct mechanical measurement of the tensile strength and elastic modulus of multiwalled carbon nanotubes. Mater Sci Engng A 2002;334(1–2):173–8.
[212] Treacy MM et al. Exceptional high Young's modulus observed for individual carbon nanotubes. Nature 1996;381(6584): 678.

[213] Poncharal P et al. Electrostatic deflections and electromechanical resonances of carbon nanotubes. Science 1999;283(5047): 1513–6.
[214] Cuenot S et al. Measurement of elastic modulus of nanotubes by resonant contact atomic force microscopy. J Appl Phys 2003;93(9):5650–5.
[215] Salvetat JP et al. Elastic and shear moduli of single-walled carbon nanotube ropes. Phys Rev Lett 1999;82(5):944–7.